JOURNAL OF PETROLOGY | VOLUME 42 | NUMBER 9 | PAGES 1643–1683 | 2001

Petrology and Geochemistry of the Lamongan Volcanic Field, East Java, Indonesia: Primitive Sunda Arc Magmas in an Extensional Tectonic Setting?

S. A. CARN* AND D. M. PYLE

DEPARTMENT OF EARTH SCIENCES, CAMBRIDGE UNIVERSITY, DOWNING STREET, CAMBRIDGE CB2 3EQ, UK

RECEIVED SEPTEMBER 30, 1999; REVISED TYPESCRIPT ACCEPTED FEBRUARY 26, 2001

New geochemical data are presented from prehistoric and historical eruptive products of the Lamongan volcanic field (LVF), East Java; a region of the Sunda arc covering $\sim$*260 km*^{2} *and containing* $\sim$*90 eruptive vents plus the historically active Lamongan volcano. LVF lavas include medium-K basalts and basaltic andesites from historical eruptions of Lamongan and prehistoric eruptions in the eastern LVF, along with a high-K suite represented by prehistoric deposits in the western LVF. Although lacking some of the characteristics of truly primary basalts, the least evolved lavas identified in the LVF have some of the lowest* SiO_2 *contents (*$\sim$*43 wt %* SiO_2*) yet reported in Sunda arc volcanic rocks. Mass balance considerations indicate that two chemically distinct LVF magmas may be parental to suites currently being erupted from the neighbouring volcanoes, Semeru and Bromo. Lamongan's historical lavas can be related to the medium-K andesitic products of Semeru by fractional crystallization, despite the former's location at the same distance from the trench as Bromo, a high-K volcano. Extensional tectonics, possibly related to arc segmentation in the region of the LVF, creating conditions that promote the rapid ascent of parental magmas, is probably responsible for this and several other features of the complex.*

KEY WORDS: *geochemistry; primitive magmas; Sunda arc; volcanic field; extensional tectonics*

INTRODUCTION

The generation and subsequent evolution of magma in subduction zone settings is widely acknowledged to be a multifarious process, involving possible inputs from the subducted oceanic lithosphere, subducted oceanic sediments and fluids, the asthenospheric and lithospheric portions of the mantle wedge above the subduction zone, and the arc crust (e.g. Tatsumi & Eggins, 1995). Following melt generation, processes such as crystal fractionation, accumulation and crustal assimilation during transit to the surface may obscure the true nature of the magma source region. The effects of these processes on the compositions of erupted lavas must therefore be removed before models of arc magma genesis can be tested.

For this reason it is desirable to sample magmas that have suffered minimal modification since segregation from their source region. The compositions of the primary or primitive magmas from different arcs provide a window on the diverse mechanisms of, and the components involved in, melt production at convergent margins, and as such are essential to our understanding of the subduction zone environment.

Many studies have highlighted the correlation between extensional tectonics in volcanic arcs and the eruption of lavas with primitive chemical characteristics (e.g. Luhr & Carmichael, 1981; Knittel & Oles, 1995; Bacon *et al.*, 1997; Smith *et al.*, 1997). In such settings, the development of thinned and fractured crust allows rising magma to erupt at the surface in a relatively unmodified state, rather than ponding at the crust–mantle boundary. The rapid passage to the surface of individual magma batches inhibits the formation of long-lived crustal magma chambers, and invariably leads to the formation of monogenetic vent fields comprising tens to thousands of individual

*Corresponding author. Present address: JCET, University of Maryland, Baltimore, MD 21250, USA. E-mail: Simon@jcet.umbc.edu

eruptive centres (such as cinder cones and maars) in these environments [e.g. the Michoacán–Guanajuato Volcanic Field, Mexico (Luhr, 1997) and the Macolod Corridor, Philippines (Knittel & Oles, 1995)].

The Sunda arc in Indonesia is a mature island arc with several structural features indicative of an active extensional regime at certain points along its length, such as developing back-arc basins (e.g. the Madura Basin, East Java; Hamilton, 1979; Fig. 1). Furthermore, the present seismic strain field beneath the volcanic arc on Java is indicative of extension oriented at a high angle to the arc, a feature common to many convergent margins (Apperson, 1991). However, there have been few documented studies of monogenetic vent fields on the Sunda arc, which, as discussed above, are also symptomatic of intra-arc extension.

This paper presents the results of a petrological and geochemical investigation of the Lamongan volcanic field (LVF) in East Java, which encompasses the historically active Lamongan volcano along with numerous cinder cones and maars (Carn, 2000). The surrounding region contains at least five recently active volcanoes (Fig. 1). The LVF sample suite covers most of the exposed vents and lava flows, and allows the characterization of the most primitive magmas in the complex. Modelling of fractional crystallization is used to place these lavas in a local and regional context. The data are also used to make preliminary judgements on the mechanisms of magma genesis in this part of the Sunda arc and on the possible effects of the regional tectonic regime on volcanism in the area.

OVERVIEW OF LAMONGAN VOLCANO AND THE LVF

Tectonic and geological setting

Lamongan volcano (8·00°S, 113·34°E; altitude 1651 m) lies on the Sunda arc between the massifs of Tengger–Semeru and Iyang–Argapura, around 200 km above the Wadati–Benioff Zone (Fig. 1). Its location corresponds to one of the narrowest sections of the island of Java, and graben structures in the vicinity of the LVF suggest local extension (Carn, 1999). The region has been little studied, and prior petrological studies are only cursory (Mulyana, 1989). The occurrence of three seismic crises in the area during the 20th century, each entailing the formation of east–west- and ENE–WSW-oriented tensional fractures on Lamongan's western flanks (Matahelumual, 1990), led to the establishment of an observatory to monitor the volcano.

The Sunda arc extends from the Andaman Islands north of Sumatra to the island of Alor in the Banda Sea over a distance of >3000 km, and incorporates 76% of Indonesia's Holocene volcanoes (Simkin & Siebert, 1994). Along much of the arc Indian Ocean crust is subducting beneath the Eurasian plate at a rate of ~6 cm/yr (Hamilton, 1979), with the downgoing slab probably continuous from the surface to the lower mantle beneath Java (Puspito & Shimazaki, 1995; Widiyantoro & van der Hilst, 1996, 1997). This continuous slab is compatible with a regional subduction history that dates back to the Permian (Katili, 1975).

The Indian Ocean crust ages eastwards along the arc (Fig. 1), being around 130–135 Ma old south of Java (Widiyantoro & Hilst, 1996). In the eastern Sunda arc, the incursion of continental crust and crustal fragments on the Indo-Australian plate complicates the system (Fig. 1). East of Flores the progressive docking of Australian continental lithosphere onto the Banda arc since the Neogene (e.g. Rangin *et al.*, 1990) has led to a cessation of volcanism at the arc front. This arc–continent collision is also believed to be responsible for incipient back-arc thrusting (from Bali eastwards; Fig. 1) and extensional features on the arc (e.g. Silver *et al.*, 1983; Charlton, 1991).

The Sunda arc has existed in roughly its current configuration for around 5 m.y., although an active volcanic arc has probably persisted in the region since at least the Eocene (Katili, 1975; Hamilton, 1979; Rangin *et al.*, 1990). The Quaternary volcanoes generally overlie Late Miocene–Pliocene volcanic rocks and sediments (Soeria-Atmadja *et al.*, 1994). The changing nature of the arc crust, from continental in Sumatra to transitional in Java and oceanic in Flores, gives rise to along-arc variation in the style and composition of volcanism (Whitford *et al.*, 1979). Silicic volcanism and large calderas (e.g. Lake Toba) on Sumatra give way to mafic–intermediate volcanism on Java, where the crust is of near-continental thickness but comprises mélanges and mafic–intermediate plutons. From Bali to Sumbawa (Fig. 1) a mature oceanic island arc has developed (Hamilton, 1988). Across-arc geochemical variations, primarily in K and $^{87}Sr/^{86}Sr$, have also been documented (Whitford & Nicholls, 1976; Whitford *et al.*, 1979).

Lamongan volcano and the LVF

Lamongan volcano is the only historically active vent in the LVF, a region covering some 260 km^2 occupied by numerous prehistoric eruptive centres including around 61 cinder cones and 29 maars (Fig. 2). Two prehistoric vents, Gunung Tarub and Gunung Tjupu, complete the central edifice (Lamongan–Tarub–Tjupu or LTT) of which Lamongan forms the southwestern segment (Figs 2 and 3). Carn (2000) presented an analysis of the physical aspects of the LVF, and his compilation of volumetric data for the cinder cones, maars and lava flows of the complex is given in Table 1. The number of vents in the

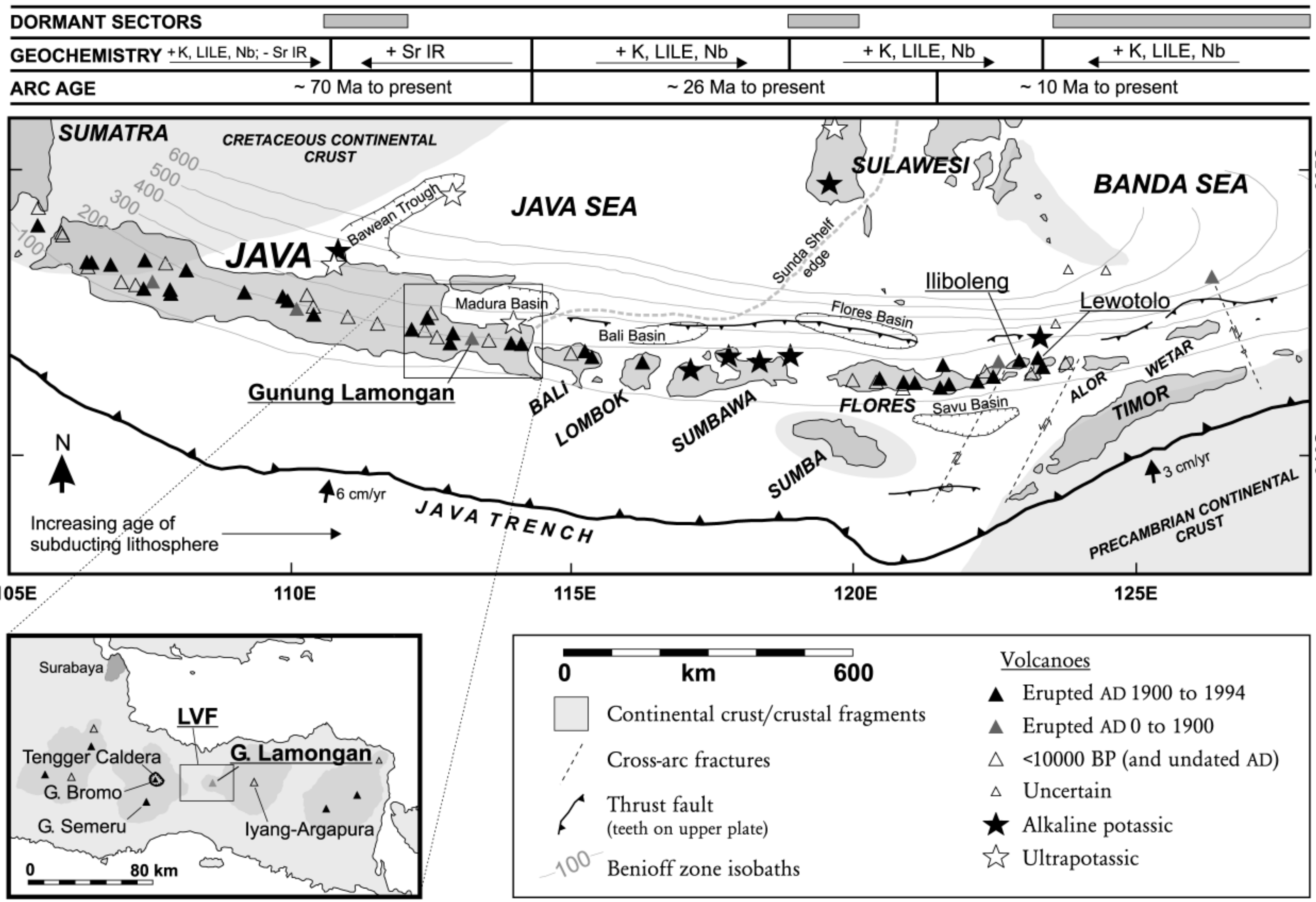

Fig. 1. Map of the eastern Sunda arc showing major tectonic features, the distribution of volcanism (including Gunung Lamongan and the LVF), and some major geochemical trends along the arc (+, increase; −, decrease in direction of arrow; Sr IR, $^{87}Sr/^{86}Sr$). Distribution of potassic and ultrapotassic volcanism in Java and Sulawesi (of Tertiary and Quaternary age) from Leterrier *et al.* (1990); other volcanoes from Simkin & Siebert (1994). Compiled from Whitford (1975), Hamilton (1979), Chotin *et al.* (1980), Foden & Varne (1980), Foden (1983), Silver *et al.* (1983), Varne (1985), Wheller *et al.* (1987), Van Bergen *et al.* (1989), Varekamp *et al.* (1989) and Edwards *et al.* (1993).

Table 1: Summary of juvenile magma volume estimates for LVF cones, lava flows and maars; from Carn (2000)

	Sample size	Volume (km^3)
Cinder or spatter cones	36	1·50
Maars	22	0·21
Prehistoric lava flows	11	0·11
Lamongan–Tarub–Tjupu	1	10·14
Lamongan eruptions (1799–1898)	10	0·049
Total		~12

LVF is exceptional for an Indonesian volcano, exceeding the 35 scoria cones reported from Gunung Slamet in central Java (Vukadinovic & Sutawidjaja, 1995), although it is somewhat fewer than that observed in larger cinder cone fields elsewhere (e.g. Mexico; Luhr, 1997). Vent distributions in the LVF suggest a strong regional tectonic influence on prehistoric volcanism in the field, which may have involved fissure-style eruptions (Carn, 1999, 2000).

Lamongan's first recorded historical activity occurred in 1799. This heralded ~100 years of unrest during which the volcano erupted up to 15 lava flows, the last in 1898 (Matahelumual, 1990; Said, 1992; Simkin & Siebert, 1994). The steady-state eruptive rate at Lamongan from 1843 to 1898 was ~0·03 m^3/s, and the age of the volcano has been estimated at 13–40 ka, assuming a constant time-averaged eruptive rate over its lifetime (Carn, 2000). With the exception of seismic crises on the volcano's flanks in 1925, 1978, 1985 and 1988–1989 (Matahelumual, 1990), Lamongan has been dormant since 1898.

FIELD OBSERVATIONS AND SAMPLING

The LVF is situated ~8° south of the equator and much of the field is well vegetated. All the observed lava flows in the LVF (historical and prehistoric) are of a'a, and are several metres thick and up to 2–3 km long (Fig. 3). Cross-sections of individual prehistoric flows, ~10–30 m thick, were found in outlying stream sections and in the vertical walls of maar craters although they often proved difficult to trace beyond these isolated exposures. Several of the dry maars were observed to contain small cinder cones (Fig. 2) indicating a sustained eruption of magma following maar formation.

The sample suite collected from the LVF is representative of most of the eruptive units and monogenetic vents in the complex (Figs 2 and 3). Samples were categorized as: (1) historical lavas (erupted from Lamongan volcano, 1799–1898); (2) cinder or spatter cones [including lava flows clearly associated with cones (mapped in Fig. 2) and cones within maars]; (3) prehistoric lava flows (flows not covered by the two preceding categories); (4) maar deposits (Table 2). No particular genetic relationships between samples in each group are implied by this classification. Samples were further subdivided on the basis of vent morphology and location, as detailed in a later section. The majority of LVF lavas are basalts and basaltic andesites, with subordinate picrobasalts, basanites, trachybasalts and trachyandesites (Table 2).

Samples from cinder or spatter cones were invariably scoriae or spindle bombs found close to the surface. Dense vegetation in the SE of the region precluded detailed exploration, but there is little evidence for young vents in this area (Bronto *et al.*, 1986). Maar deposits were poorly preserved and juvenile material was difficult to identify. The provenance of maar samples is hence largely unknown; some material may have been reworked by the disruption of subsurface lava flows. For comparison, several new analyses from volcanoes adjacent to the LVF (Semeru and Bromo) are also presented (Fig. 1; Table 2).

ANALYTICAL TECHNIQUES

Whole-rock samples were analysed for major and trace elements by X-ray fluorescence (XRF) at the Open University, Milton Keynes, on an ARL 8420+ wavelength-dispersive XRF spectrometer. Fresh cores of lavas were washed in deionized water and dried before crushing in an agate grinder. Pressed powder pellets for trace element determination were prepared in Cambridge, and fused glass discs for major element analyses were prepared in Milton Keynes. Data quality was monitored by running in-house igneous rock standards with each sample batch. Trace element detection limits are given in Table 2. Mineral analyses were performed on carbon-coated polished slides using a Cameca SX-50 electron microprobe in Cambridge. Analytical conditions were a 10 kV accelerating voltage, beam currents of 4–15 nA and a beam diameter of 5 μm; all analyses were energy dispersive. Precision, monitored using various standards, is generally within 1–2% for major elements. To determine Sr isotopic ratios, ~150 mg aliquots of rock powder were dissolved in $HF–HNO_3$ and the resulting solution was evaporated until dry. After further dissolution in HNO_3 the solution

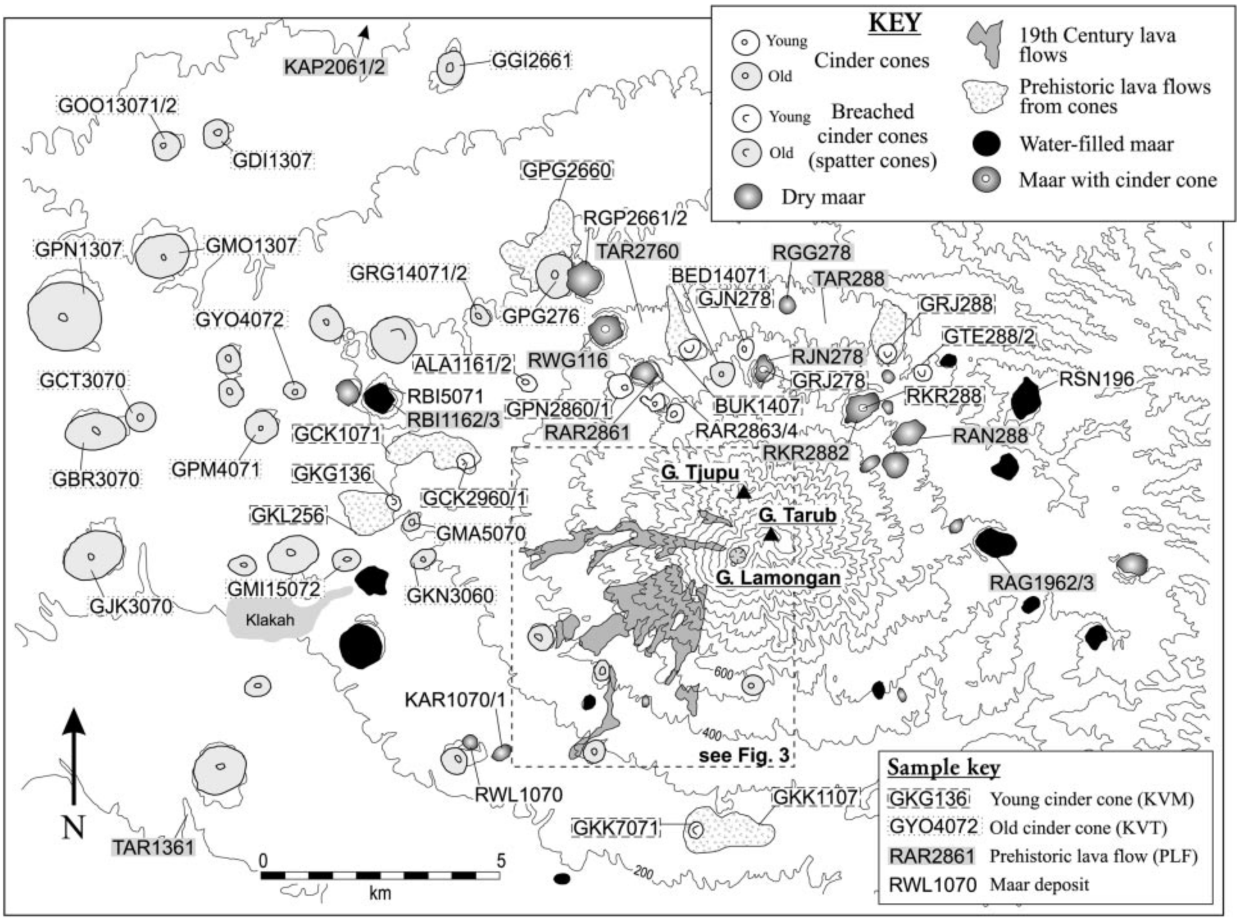

Fig. 2. Map of the LVF showing the monogenetic vents and lava flows, and the distribution of samples used in this study. Cinder cones are classified as either 'young' (KVM series) or 'old' (KVT series) according to the morphological criteria of Carn (2000). Dashed box indicates the location of Fig. 3. Contour interval is 100 m, except for supplementary contours on some cinder cones. Contours on the east edge of the map mark the western flanks of the Iyang–Argapura massif (Fig. 1). Derived partly from Bronto *et al.* (1986).

was evaporated again; the samples were then redissolved in HCl. After centrifuging, samples were loaded onto cation-exchange resin and Sr was eluted using HCl. The dried residue was loaded in HCl onto an outgassed Ta filament and analysed on a VG Sector 54 mass spectrometer in Cambridge. Ratios were corrected for mass fractionation by normalizing to $^{86}Sr/^{88}Sr = 0{\cdot}1194$. Repeat analyses of NBS 987 gave a mean value of 0·710263.

PETROGRAPHY

Historical lavas

Historical lavas from Lamongan volcano typically contain phenocrysts of plagioclase (*Plag*), clinopyroxene (*Cpx*), olivine (*Ol*) and Ti-magnetite (*Mag*) in a crystal-rich, seriate-textured groundmass with similar mineralogy and variable amounts of glass (often devitrified). The petrography of the lavas is generally rather uniform throughout the series. Modal analyses (point-counted) for 10 historical lavas are listed in Table 3.

Subhedral *Plag* is the predominant phase in all samples, accounting for up to 70% of the modal mineralogy (Table 3). It typically occurs as complex aggregates or glomerocrysts (up to 3–4 mm square; associated with *Cpx* and *Mag*), and often exhibits fine-scale concentric zoning, sieve texture and resorption features (e.g. embayed rims), and zoned inclusions suggesting a complex history. Microphenocrysts often show similar features. Inclusions of pyroxene and *Mag* are often observed in *Plag*. Groundmass alignments of *Plag* are rarely observed and are never well developed. Phenocrysts range up to 3–4 mm in size.

Cpx also occurs in aggregates (with *Plag*, Fe–Ti oxides and *Ol*), although less frequently than *Plag*. It is typically subhedral, concentrically zoned, and occasionally displays twin lamellae; phenocrysts are up to ~2 mm in size.

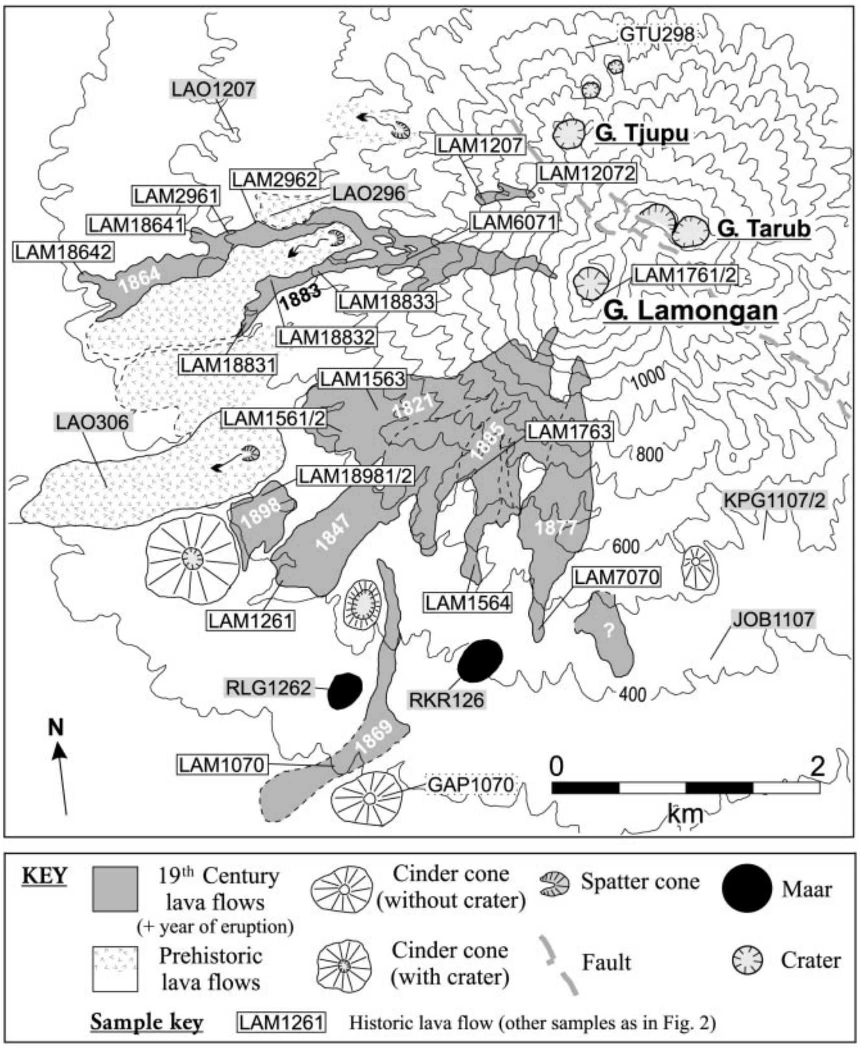

Fig. 3. Map of the flanks of Lamongan volcano showing the lava flow field emplaced during 19th-century activity (from Carn, 2000). The provenance of samples used in this study is indicated. Eruption dates are reasonably well constrained from historical records (e.g. Matahelumual, 1990), although these are less reliable for the older flows.

Embayed and sieve-textured *Cpx* (and rare skeletal grains) is also present in some samples. Inclusions of *Plag* are rare, but zones of Fe–Ti oxide inclusions are frequent; a common texture observed in the historical lavas (and in other samples; see below) is the mantling of *Cpx* phenocrysts by small Fe–Ti oxide crystals. Low-Ca pyroxene is present only as a minor phase in the more evolved lavas (e.g. LAM1561). It occurs as resorbed crystal cores or as rims enveloping *Cpx* phenocrysts.

Ol is typically less abundant than *Plag* and *Cpx* in the historical lavas (Table 3). It occurs as phenocrysts (up to 1 mm across) and microphenocrysts (generally <0·5 mm across) that are frequently embayed, and it is also present in the groundmass of several samples.

Also observed in several samples (e.g. LAM18981, LAM18831, LAM1070) are clots or nodules containing *Plag*, *Cpx*, *Mag* and occasional *Ol*, up to 0·8 mm in size. The pyroxene in these clots is generally unzoned and often shows a subophitic or ophitic texture, distinguishing them from the ubiquitous glomerocrysts that have similar constituents. Several nodules show disequilibrium features such as sieve-texture and resorbed boundaries. These nodules are interpreted as cumulate material derived from the edges of an evolving magma chamber.

Plag glomerocrysts are less common in the younger lavas (LAM18982, LAM18832; Table 3), suggesting that a flotation mechanism (e.g. Campbell *et al.*, 1978) may

Table 2: Analyses of historical lava flows, cinder and scatter cones, prehistoric lava flows and maar deposits of the LVF

	Historical lava flows of the LVF											
Sample no.:	LAM18981	LAM18982	LAM18831	LAM18832	LAM18833	LAM18641	LAM18642	LAM1261	LAM1561	LAM1562	LAM1563	LAM1564
Locality:	1898 flow G. Anyar	1898 flow G. Anyar	1883 flow Bertjak	1883 flow Bertjak	1883 flow Bertjak	1864 flow Anter	1864 flow Anter	1847 flow SE G. Kenek	1821 flow NE G. Anyar	1821 flow NE G. Anyar	1821 flow NE G. Anyar	1885 flow N R. Kambang
Rock type:	a'a lava	a'a lava	a'a lava	a'a lava	a'a lava	a'a lava	a'a lava	a'a lava	a'a lava	a'a lava	a'a lava	a'a lava
SiO_2	47·81	47·97	49·70	51·00	51·04	51·02	51·14	52·81	54·59	54·43	51·52	51·03
TiO_2	1·100	1·103	1·044	0·979	0·962	0·953	0·973	0·916	0·841	0·840	0·939	0·962
Al_2O_3	19·68	19·69	19·64	19·43	19·39	19·56	19·43	18·35	19·60	19·67	19·03	19·63
Fe_2O_3*	12·00	12·01	11·63	11·50	11·41	11·28	11·42	10·71	9·59	9·53	10·81	11·16
MnO	0·191	0·190	0·189	0·198	0·197	0·196	0·202	0·207	0·208	0·208	0·190	0·196
MgO	5·15	5·16	4·56	4·22	4·27	4·10	4·19	4·14	2·85	2·79	4·27	4·04
CaO	11·06	11·10	9·83	9·33	9·44	9·27	9·40	8·86	8·13	8·13	9·29	9·24
Na_2O	2·65	2·67	3·03	3·15	3·14	3·20	3·15	3·39	3·74	3·74	3·26	3·23
K_2O	0·68	0·67	0·88	0·92	0·91	0·93	0·93	1·10	1·09	1·08	1·00	0·98
P_2O_5	0·122	0·117	0·171	0·177	0·179	0·183	0·178	0·220	0·230	0·225	0·199	0·189
LOI	−0·43	−0·46	−0·45	−0·49	−0·56	−0·43	−0·48	−0·30	−0·35	−0·30	−0·33	−0·47
Total	100·01	100·22	100·22	100·41	100·38	100·26	100·53	100·40	100·52	100·34	100·18	100·19
FeOt	7·49	7·46	n.d.	7·84	7·68	n.d.	7·67	7·21	n.d.	6·36	7·15	n.d.
Fe_2O_3t	3·68	3·72	n.d.	2·79	2·87	n.d.	2·90	2·70	n.d.	2·46	2·86	n.d.
mg-no.	0·553	0·555	n.d.	0·492	0·500	n.d.	0·496	0·508	n.d.	0·441	0·518	n.d.
Rb	9·9	9·5	12·9	14·8	13·8	14·4	13·7	17·4	17·9	17·3	15·6	15·0
Sr	376	376	397	398	397	400	396	386	467	465	392	394
Y	20·7	21·0	22·7	23·3	23·1	24·0	24·4	27·4	25·9	25·5	25·5	23·1
Zr	44	44	61	65	62	65	61	75	75	74	69	67
Nb	1·5	b.d.	1·6	2·5	2·6	1·7	1·7	2·1	2·3	2·3	2·7	1·9
Ba	335	333	427	429	414	435	408	504	501	505	473	449
Pb	b.d.	6	7	6	b.d.	5	6	7	7	7	6	7
Th	6	4	b.d.	b.d.	4	b.d.	b.d.	b.d.	b.d.	b.d.	b.d.	b.d.
U	b.d.	b.d.	b.d.	b.d.	b.d.	b.d.	b.d.	b.d.	b.d.	b.d.	b.d.	b.d.
Sc	31	33	30	26	23	23	23	28	20	15	23	24
V	409	407	324	278	275	267	274	242	124	132	277	260
Cr	9	6	9	8	8	5	8	11	6	6	10	7
Co	37	36	33	29	30	30	30	27	19	17	27	30
Ni	6	7	6	4	3	7	4	6	b.d.	5	6	7
Cu	77	76	68	55	56	53	56	43	29	31	48	61
Zn	87	86	90	92	85	91	85	88	85	83	82	94
Ga	19	18	19	19	21	19	18	18	17	18	19	18
K (ppm)	5643	5560	7302	7634	7551	7717	7717	9128	9045	8962	8298	8132
$^{87}Sr/^{86}Sr$	n.d.	0·70432	0·7042	n.d.	n.d.	n.d.	n.d.	n.d.	0·70433	n.d.	n.d.	n.d.
IUGS class.	MKSB	MKSB	MKSB	MKSB	MKSB	MKSB	MKSB	MKBA	MKBA	MKBA	MKSB	MKSB

Table 2: continued

	Historical lava flows of the LVF									
Sample no.:	LAM2961	LAM2962	LAM6071	LAM7070	LAM1070	LAM1207	LAM12072	LAM1761	LAM1762	LAM1763
Locality:	1864 flow Anter	1864 flow Anter	1883 flow W Lamongan	1877 flow Darungantimur	1869 flow Salaktengah	historic flow NW Lamongan	historic flow NW Lamongan	summit crater Lamongan	summit crater Lamongan	1885 flow SW Lamongan
Rock type:	a'a lava	a'a lava	a'a lava	a'a lava	a'a lava	a'a lava	a'a lava	lava block	lava block	a'a lava
SiO_2	50·88	51·18	49·71	50·19	50·13	54·56	49·53	49·78	50·92	49·89
TiO_2	0·953	0·954	1·042	0·972	1·004	0·914	1·027	1·063	0·985	1·064
Al_2O_3	19·54	19·72	19·69	19·86	19·45	18·90	19·64	19·03	19·53	19·20
Fe_2O_3*	11·27	11·19	11·61	11·17	11·63	10·07	11·60	11·74	11·40	11·66
MnO	0·195	0·194	0·192	0·186	0·194	0·232	0·191	0·204	0·196	0·205
MgO	4·13	3·99	4·53	4·44	4·62	2·93	4·54	4·58	4·30	4·53
CaO	9·28	9·34	9·81	9·74	9·81	7·82	9·70	10·41	9·54	10·40
Na_2O	3·18	3·18	3·02	3·16	3·04	3·68	3·05	2·99	3·13	3·01
K_2O	0·93	0·91	0·87	0·91	0·87	1·05	0·87	0·78	0·90	0·79
P_2O_5	0·182	0·177	0·170	0·182	0·170	0·227	0·169	0·144	0·174	0·152
LOI	−0·31	−0·54	−0·45	−0·53	−0·40	−0·40	−0·18	−0·47	−0·54	−0·53
Total	100·23	100·30	100·19	100·28	100·52	99·98	100·14	100·25	100·54	100·37
FeOt	n.d.	7·31	n.d.	7·42	7·40	6·92	5·23	n.d.	7·17	8·02
Fe_2O_3t	n.d.	3·07	n.d.	2·92	3·41	2·38	5·79	n.d.	3·43	2·75
mg-no.	n.d.	0·496	n.d.	0·519	0·529	0·433	0·610	n.d.	0·519	0·504
Rb	14·2	13·4	13·3	13·9	11·8	18·2	12·5	11·3	13·0	11·0
Sr	403	401	391	400	392	478	392	381	398	388
Y	22·9	23·1	22·3	22·7	22·9	27·1	22·2	22·8	22·5	22·8
Zr	66	65	58	59	60	73	60	54	60	54
Nb	1·8	1·6	2·1	b.d.	2·2	2·4	b.d.	2·2	1·5	2·1
Ba	419	414	396	443	416	486	429	397	439	400
Pb	5	b.d.	6	b.d.	6	6	b.d.	b.d.	7	b.d.
Th	b.d.	b.d.	b.d.	b.d.	b.d.	b.d.	b.d.	b.d.	b.d.	b.d.
U	b.d.	b.d.	b.d.	b.d.	b.d.	b.d.	b.d.	b.d.	b.d.	b.d.
Sc	21	22	29	26	30	14	31	29	23	29
V	271	265	325	305	316	99	315	324	292	319
Cr	8	7	8	9	8	6	10	6	10	7
Co	28	32	32	33	31	16	33	28	28	28
Ni	6	5	6	7	7	b.d.	7	6	6	b.d.
Cu	54	57	70	57	73	18	67	59	23	65
Zn	90	87	87	85	88	84	87	80	80	89
Ga	19	18	20	18	19	18	18	19	18	20
K (ppm)	7717	7551	7219	7551	7219	8713	7219	6472	7468	6555
$^{87}Sr/^{86}Sr$	n.d.	n.d.	n.d.	n.d.	n.d.	n.d.	n.d.	n.d.	n.d.	n.d.
IUGS class.	MKSB	MKSB	MKSB	MKSB	MKSB	MKBA	MKSB	MKSB	MKSB	MKSB

	Cinder and scatter cones of the LVF											
Sample no.:	ALA1161	ALA1162	GCK1071	GCK2960	GCK2961	GKG136	GKL256	GMA5070	GMI15072	GKN3060	GKK1107	GKK7071
Locality:	Alun-alun cinder cone	Alun-alun cinder cone	G. Cilik lava flow	G. Cilik spatter cone	G. Cilik spatter cone	G. Kendeng spatter cone	G. Kendeng lava flow	G. Meja cone	G. Matruki cone	G. Kemaran lava flow	G. Kenek [S] lava flow	G. Kenek [S] spatter cone
Rock type:	scoria	scoria	lava block	lava block	scoria	scoria	lava block	lava block	lava block	lava block	lava block	lava bomb
Series:	KVM	KVM	KVM	KVM	KVM	KVM	KVM	KVT	KVT	KVT	KVM	KVM
SiO_2	44·64	44·33	44·87	50·91	45·32	45·32	46·35	45·04	51·78	46·16	44·32	44·66
TiO_2	1·514	1·502	1·231	0·947	1·219	1·213	1·162	1·249	1·139	1·098	1·484	1·486
Al_2O_3	18·23	18·16	18·07	19·65	17·65	17·30	18·17	17·46	17·62	20·21	17·93	18·02
Fe_2O_3*	14·31	14·33	13·76	10·74	13·50	13·06	12·88	13·33	10·80	12·01	14·45	14·34
MnO	0·190	0·192	0·195	0·186	0·193	0·188	0·194	0·187	0·184	0·191	0·188	0·191
MgO	6·40	6·37	6·63	4·27	6·96	7·20	6·44	7·37	4·84	5·06	6·61	6·52
CaO	12·68	12·59	12·08	9·64	12·42	12·83	12·23	12·73	9·16	11·62	12·66	12·69
Na_2O	2·15	2·15	2·09	3·21	2·21	1·93	2·36	2·05	2·84	2·51	2·16	2·26
K_2O	0·64	0·64	1·15	0·95	1·19	0·86	0·94	0·88	1·30	1·3	0·62	0·65
P_2O_5	0·081	0·079	0·196	0·188	0·181	0·146	0·167	0·158	0·228	0·198	0·077	0·080
LOI	−0·27	−0·23	0·07	−0·37	−0·38	−0·07	−0·52	−0·21	−0·09	−0·37	−0·47	−0·58
Total	100·57	100·11	100·34	100·32	100·46	99·98	100·37	100·24	99·80	99·99	100·03	100·32
FeOt	7·17	n.d.	n.d.	6·92	n.d.	n.d.	8·11	n.d.	n.d.	n.d.	9·12	n.d.
Fe_2O_3t	6·34	n.d.	n.d.	3·05	n.d.	n.d.	3·87	n.d.	n.d.	n.d.	4·31	n.d.
mg-no.	0·616	n.d.	n.d.	0·526	n.d.	n.d.	0·588	n.d.	n.d.	n.d.	0·566	n.d.
Rb	6·7	6·3	33·9	15·2	33·2	22·7	25·0	21·4	31·2	35·4	7·8	8·1
Sr	358	357	432	405	418	375	413	382	394	474	328	332
Y	20·2	19·8	21·6	23·7	21·7	19·5	21	19·9	31·1	20·3	19·9	19·8
Zr	27	26	40	61	40	34	38	34	101	41	29	31
Nb	1·7	1·6	3·2	2·6	3·3	2·4	1·7	3·2	3·6	2	1·8	2·5
Ba	283	280	315	447	299	238	278	252	622	314	282	284
Pb	b.d.	b.d.	7	5	b.d.	b.d.	5	5	7	6	b.d.	b.d.
Th	b.d.	b.d.	4	b.d.	5	b.d.	b.d.	b.d.	4	4	b.d.	b.d.
U	b.d.	b.d.	b.d.	b.d.	b.d.	b.d.	b.d.	b.d.	b.d.	b.d.	b.d.	b.d.
Sc	47	39	42	26	41	51	41	50	31	26	45	42
V	578	573	472	276	469	483	445	507	293	393	579	587
Cr	9	10	44	10	61	37	23	45	37	13	9	8
Co	43	41	44	27	44	43	41	47	37	39	40	45
Ni	8	8	19	7	20	16	13	20	26	11	9	8
Cu	90	87	86	54	92	82	86	84	144	104	86	84
Zn	72	73	86	79	87	80	78	78	92	85	75	74
Ga	17	17	17	19	15	17	18	16	19	18	17	18
K (ppm)	5311	5311	9543	7883	9875	7136	7800	7302	10787	10787	5145	5394
$^{87}Sr/^{86}Sr$	0·70428	n.d.	n.d.	n.d.	0·70445	n.d.	n.d.	n.d.	n.d.	n.d.	0·70438	n.d.
IUGS class.	PB	PB	SB	MKSB	SB	SB	SB	SB	MKBA	SB	PB	PB

Table 2: continued

	Cinder and scatter cones of the LVF											
Sample no.:	GPG276	GPG2660	GPN2860	GPN2861	GGI2661	GRG14071	GRG14072	BED14071	BUK1407	GCT3070	GBR3070	GPN1307
Locality:	G. Parang cone	G. Parang lava Kramat	G. Pandan cone	G. Pandan cone	G. Geni Kali Cicaluk	G. Rindang lava flow	G. Rindang cone	G. Bedian cone	G. Bukor lava flow	G. Ciut cone	G. Blingir cone	G. Panawungan cone
Rock type:	scoria	a'a lava	scoria	scoria	lava bomb	lava block	lava bomb	lava block	a'a lava	scoria	scoria	lava bomb
Series:	KVT	KVM	KVM	KVM	KVT	KVT	KVT	KVT	KVM	KVT	KVT	KVT
SiO_2	44·52	44·40	44·52	47·31	45·48	50·97	54·28	49·99	45·57	51·15	52·71	55·58
TiO_2	1·474	1·479	1·428	1·281	1·415	0·947	0·925	0·889	1·381	1·219	1·577	1·363
Al_2O_3	18·01	17·89	18·03	20·08	18·38	19·72	18·85	17·38	18·61	17·5	16·73	15·74
Fe_2O_3*	14·34	14·41	13·85	12·64	13·78	10·68	10·08	10·78	13·35	11·49	12·11	11·34
MnO	0·187	0·188	0·190	0·207	0·195	0·186	0·227	0·178	0·199	0·199	0·194	0·210
MgO	6·57	6·63	6·58	4·57	6·06	4·13	2·93	6·50	5·81	5·27	3·76	2·70
CaO	12·76	12·86	12·79	10·38	12·10	9·53	7·79	10·31	12·33	9·23	7·76	6·63
Na_2O	2·24	2·20	2·22	3·19	2·33	3·19	3·65	2·58	2·41	2·58	3·21	3·54
K_2O	0·65	0·65	0·66	0·94	0·62	0·97	1·06	1·25	0·67	0·95	1·81	2·19
P_2O_5	0·082	0·078	0·069	0·097	0·083	0·199	0·226	0·207	0·107	0·292	0·411	0·391
LOI	−0·50	−0·59	−0·44	−0·38	−0·46	−0·26	−0·14	0·31	−0·51	−0·34	−0·06	0·45
Total	100·33	100·20	99·90	100·32	99·98	100·26	99·88	100·37	99·93	99·54	100·21	100·13
FeOt	n.d.	8·89	n.d.	6·22	7·99	n.d.	n.d.	n.d.	7·58	n.d.	n.d.	n.d.
Fe_2O_3t	n.d.	4·53	n.d.	5·73	4·90	n.d.	n.d.	n.d.	4·93	n.d.	n.d.	n.d.
mg-no.	n.d.	0·573	n.d.	0·569	0·577	n.d.	n.d.	n.d.	0·580	n.d.	n.d.	n.d.
Rb	8·1	7·6	7·2	10·5	6·1	14·0	18	22·5	8·0	25·0	n.d.	59·9
Sr	324	329	325	408	347	409	479	519	382	434	n.d.	344
Y	19·6	19·5	19·2	22·5	20·1	23·8	26·6	18·3	20·4	32·2	n.d.	44·1
Zr	27	30	30	39	33	62	71	47	32	109	n.d.	165
Nb	1·5	1·7	1·8	b.d.	b.d.	3	2·3	1·8	b.d.	4·4	n.d.	7·2
Ba	276	278	277	411	304	452	482	415	313	559	n.d.	1006
Pb	b.d.	b.d.	6	b.d.	b.d.	b.d.	6	6	b.d.	11	n.d.	15
Th	b.d.	b.d.	b.d.	b.d.	b.d.	b.d.	b.d.	5	b.d.	4	n.d.	9
U	b.d.	b.d.	b.d.	b.d.	b.d.	b.d.	b.d.	b.d.	b.d.	b.d.	n.d.	b.d.
Sc	45	49	44	24	41	27	14	34	36	34	n.d.	31
V	609	599	573	374	520	271	101	303	460	292	n.d.	183
Cr	7	9	41	4	7	9	6	82	8	57	n.d.	6
Co	44	42	44	32	42	27	15	37	39	33	n.d.	26
Ni	11	11	12	4	6	6	4	33	6	41	n.d.	b.d.
Cu	96	97	86	70	69	43	15	163	68	144	n.d.	47
Zn	75	76	77	76	78	77	80	75	79	95	n.d.	126
Ga	15	16	17	17	17	19	16	17	16	18	n.d.	18
K (ppm)	5394	5394	5477	7800	5145	8049	8796	10372	5560	7890	15027	18172
$^{87}Sr/^{86}Sr$	n.d.	n.d.	n.d.	n.d.	0·70427	n.d.	n.d.	n.d.	n.d.	n.d.	n.d.	n.d.
IUGS class.	PB	PB	PB	SB	SB	MKSB	MKBA	MKSB	SB	MKSB	HKBA	HKBA

	Cinder and scatter cones of the LVF											
Sample no.:	GMO1307	GDI1307	GOO13071	GOO13072	RKR288	GJN278	GRJ278	GRJ288	GTE288	GTE2882	GTU298	GAP1070
Locality:	G. Mejo cone	G. Dami cone	G. Onggoonggo cone	G. Onggoonggo cone	Ranu Kembar cone/lava flow	G. Kenek [N] cone	Ranu Semungka cinder cone	G. Rojing cone	G. Tangke cone	G. Tangke lava flow	G. Tjupu cone	G. Salak cone
Rock type:	lava block	lava bomb	lava bomb	lava bomb	lava block	lava block	scoria	lava bomb	lava bomb	lava block	scoria	lava block
Series:	KVT	KVT	KVT	KVT	KVM	KVM	KVM	KVM	KVM	KVM	KVT	KVT
SiO_2	50·45	50·9	50·69	50·56	43·79	43·31	44·61	43·52	51·10	46·38	45·50	52·99
TiO_2	1·300	1·343	1·364	1·340	1·431	1·530	1·437	1·486	1·120	1·320	1·362	1·15
Al_2O_3	18·29	17·36	17·29	17·22	18·45	16·87	18·15	17·59	17·81	19·66	19·44	17·34
Fe_2O_3*	11·80	12·17	12·50	12·37	14·08	15·11	13·99	14·54	11·13	12·68	13·01	10·86
MnO	0·201	0·202	0·207	0·204	0·186	0·181	0·184	0·179	0·199	0·192	0·192	0·207
MgO	4·74	4·72	4·81	4·68	6·35	7·52	6·30	6·98	3·85	5·12	5·43	3·6
CaO	9·62	8·69	8·79	8·70	12·37	13·40	12·61	13·02	7·86	11·59	11·90	7·02
Na_2O	2·65	2·69	2·71	2·70	1·98	1·96	2·44	2·03	3·35	2·66	2·41	3·63
K_2O	1·22	1·6	1·47	1·44	0·59	0·56	0·65	0·61	2·30	0·77	0·71	2·69
P_2O_5	0·338	0·408	0·405	0·397	0·075	0·070	0·086	0·070	0·395	0·079	0·077	0·461
LOI	−0·24	−0·14	0·07	0·31	0·24	−0·54	−0·56	−0·22	0·40	−0·59	0·02	0·32
Total	100·37	99·94	100·31	99·92	99·54	99·98	99·89	99·80	99·49	99·85	100·05	100·26
FeOt	n.d.	n.d.	6·78	n.d.	n.d.	n.d.	n.d.	n.d.	n.d.	n.d.	n.d.	n.d.
Fe_2O_3t	n.d.	n.d.	4·97	n.d.	n.d.	n.d.	n.d.	n.d.	n.d.	n.d.	n.d.	n.d.
mg-no.	n.d.	n.d.	0·561	n.d.	n.d.	n.d.	n.d.	n.d.	n.d.	n.d.	n.d.	n.d.
Rb	29·1	63·4	55·5	56·4	7·1	5·8	9·1	7·8	54·8	9·9	7·4	65·4
Sr	449	385	384	381	318	297	338	308	599	386	363	560
Y	37·4	42·2	42	41	19·0	17·8	19·1	19·2	27·0	20·6	20·2	29·7
Zr	102	182	180	174	33	30	34	32	99	39	40	111
Nb	3·9	7	6·3	6·2	1·7	b.d.	2·1	1·7	6·6	1·6	3·3	9·0
Ba	618	663	691	676	283	252	285	258	796	347	342	920
Pb	8	13	17	13	b.d.	10	b.d.	5	10	5	b.d.	9
Th	5	9	10	9	b.d.	b.d.	4	b.d.	6	b.d.	4	9
U	b.d.	b.d.	b.d.	3	3	b.d.	b.d.	3	b.d.	b.d.	b.d.	b.d.
Sc	28	37	34	36	40	57	43	50	26	29	35	30
V	289	282	311	293	577	668	577	655	280	424	481	261
Cr	27	24	24	23	15	46	10	25	5	6	9	4
Co	29	32	34	37	46	51	45	52	28	36	39	26
Ni	19	17	20	21	19	22	13	22	12	11	12	15
Cu	220	137	158	172	72	132	93	119	194	74	51	139
Zn	96	113	113	116	73	68	74	77	92	70	77	95
Ga	20	18	19	20	14	15	16	18	19	15	17	18
K (ppm)	10123	13277	12198	11949	4896	4647	5394	5062	19085	6389	5892	22321
$^{87}Sr/^{86}Sr$	n.d.	n.d.	0·70433	n.d.	n.d.	n.d.	n.d.	n.d.	n.d.	n.d.	n.d.	n.d.
IUGS class.	MKSB	HKSB	MKSB	MKSB	PB	PB	BS	PB	SH	SB	SB	SH

Table 2: continued

	Cinder and scatter cones of LVF			Prehistoric lava flows of the LVF							
Sample no.:	GJK3070	GPM4071	GYO4072	RAG1962	RAG1963	RWG116	RAR2861	JOB1107	RBI1162	RBI1163	RLG1262
Locality:	G. Jalak cone	G. Pakem cone	G. Yoso cone	Ranu Agung W end of maar	Ranu Agung W end of maar	Ranu Wurung SE end of maar	Ranu Air W crater floor	Joboan S Lamongan	Ranu Bedali SW end of maar	Ranu Bedali S crater wall	Ranu Lading SW crater wall
Rock type:	lava bomb	lava block	lava block	massive lava	lava block	massive lava	lava block	lava block	lava block	massive lava	massive lava
Series:	KVT	KVT	KVT	PLF2	PLF2	PLF2	PLF2	PLF3	PLF1	PLF1	PLF2
SiO_2	52·13	50·83	50·57	45·64	47·40	47·40	46·67	44·52	50·59	50·53	47·90
TiO_2	1·601	1·783	2·008	0·948	1·137	1·053	0·878	1·488	2·047	2·052	1·222
Al_2O_3	15·98	16·34	14·84	15·66	19·28	18·89	16·37	18·13	14·77	14·74	19·38
Fe_2O_3*	13·13	13·4	15·58	12·82	13·09	12·16	12	14·18	15·65	15·66	12·67
MnO	0·205	0·196	0·249	0·193	0·199	0·199	0·193	0·188	0·254	0·252	0·206
MgO	3·94	4·18	4·15	10·95	5·62	6·53	9·98	6·39	4·2	4·21	4·88
CaO	7·6	8·25	7·8	12·2	11·03	11·04	12·33	12·72	7·85	7·88	10·70
Na_2O	2·91	2·92	2·73	1·75	2·53	2·42	1·89	2·17	2·62	2·67	2·84
K_2O	1·75	1·67	1·89	0·31	0·56	0·49	0·36	0·63	2·04	1·98	0·67
P_2O_5	0·393	0·442	0·535	0·085	0·146	0·134	0·097	0·078	0·53	0·541	0·170
LOI	−0·11	0·01	−0·39	−0·37	−0·59	−0·43	−0·46	−0·54	−0·37	−0·33	−0·42
Total	99·53	100·02	99·96	100·19	100·40	99·89	100·31	99·954	100·18	100·19	100·22
FeOt	n.d.	n.d.	n.d.	7·91	n.d.	7·19	n.d.	n.d.	n.d.	n.d.	n.d.
Fe_2O_3t	n.d.	n.d.	n.d.	4·03	n.d.	4·17	n.d.	n.d.	n.d.	n.d.	n.d.
mg-no.	n.d.	n.d.	n.d.	0·714	n.d.	0·620	n.d.	n.d.	n.d.	n.d.	n.d.
Rb	55·1	47·0	67·8	4	7·1	6·5	4·9	7·3	76·6	74·1	8·8
Sr	346	386	325	290	452	392	389	337	327	331	473
Y	42·6	47·1	57·4	15·2	19·3	19·6	15·9	20·4	57·7	58·2	21·6
Zr	173	170	224	19	36	32	24	32	226	226	40
Nb	7·6	7·5	10·1	b.d.	1·8	b.d.	b.d.	1·5	8·7	9·4	2·9
Ba	854	895	881	203	403	290	253	294	893	885	279
Pb	15	13	17	5	b.d.	b.d.	b.d.	6	20	18	6
Th	8	8	14	b.d.	4	b.d.	b.d.	b.d.	13	11	b.d.
U	b.d.	b.d.	4	b.d.	b.d.	b.d.	b.d.	b.d.	4	b.d.	b.d.
Sc	32	40	46	51	38	35	48	44	38	42	28
V	337	325	419	373	421	331	361	571	425	419	332
Cr	15	22	14	153	9	44	140	9	13	15	9
Co	35	35	35	62	44	42	52	44	35	36	32
Ni	35	31	24	59	13	21	57	11	15	12	3
Cu	182	253	231	67	161	70	100	91	252	239	60
Zn	123	107	133	76	76	78	76	75	136	144	68
Ga	19	20	21	16	18	18	16	17	20	21	17
K (ppm)	14521	13857	15683	2572	4647	4066	2987	5228	16928	16430	5560
$^{87}Sr/^{86}Sr$	n.d.	n.d.	n.d.	0·70433	n.d.	0·70433	n.d.	n.d.	n.d.	n.d.	n.d.
IUGS class.	HKBA	HKSB	HKSB	SB	SB	SB	SB	PB	HKSB	HKSB	MKSB

	Prehistoric lava flows of the LVF											
Sample no.:	LAO1207	LAO296	LAO306	TAR1361	TAR2760	KAP2061	KAP2062	KPG1107	KPG11072	RAN288	RGG278	RJN278
Locality:	E Gunturan dry river bed	E Anter flow edge	N G. Kenek flow top	Kali Grebogan Grobogan	Jambuan flow edge	K. Curahbubur Kramatbukol	K. Curahbubur Kramatbukol	K. Penggung N Joboan	K. Penggung N Joboan	Ranu Tangke S end of maar	Ranu Gedang W crater wall	Ranu Semungka W crater wall
Rock type:	massive lava	lava block	lava block	massive lava	lava block	massive lava	massive lava	massive lava	massive lava	lava block	massive lava	massive lava
Series:	PLF3	PLF3	PLF3	PLF1	PLF3	PLF1	PLF1	PLF2	PLF2	PLF2	PLF2	PLF2
SiO_2	51·92	47·34	54·57	51·41	45·78	49·97	50·91	49·77	49·52	50·80	45·92	47·19
TiO_2	0·79	1·207	0·830	1·753	1·397	1·79	1·322	0·978	0·964	0·890	1·331	1·255
Al_2O_3	19·16	20·13	19·59	16·22	18·66	15·92	17·46	20·14	20·76	19·83	19·37	20·23
Fe_2O_3*	10·9	11·7	9·45	12·95	13·43	13·3	12·27	11·09	10·72	11·10	12·78	12·45
MnO	0·244	0·202	0·205	0·200	0·2	0·209	0·201	0·203	0·195	0·213	0·196	0·204
MgO	4·00	4·67	2·74	4·22	5·85	4·35	4·67	4·41	4·1	4·06	5·22	4·39
CaO	9·56	11·51	8·04	8·39	12·37	8·85	8·66	10·19	10·34	9·44	11·56	10·36
Na_2O	2·77	2·83	3·71	2·89	2·42	2·83	2·7	2·99	2·92	3·10	2·78	3·18
K_2O	0·62	0·86	1·08	1·75	0·66	1·68	1·49	0·67	0·65	0·87	0·81	0·92
P_2O_5	0·252	0·102	0·232	0·418	0·098	0·433	0·389	0·214	0·21	0·252	0·087	0·095
LOI	−0·43	−0·34	−0·42	0·21	−0·51	0·67	0·08	−0·47	−0·18	−0·25	−0·38	−0·48
Total	99·79	100·21	100·03	100·41	100·36	100	100·15	100·19	100·2	100·30	99·68	99·79
FeOt	7·69	6·47	6·19	7·86	8·01	7·34	n.d.	n.d.	n.d.	n.d.	n.d.	n.d.
Fe_2O_3t	2·35	4·51	2·57	4·21	4·53	5·14	n.d.	n.d.	n.d.	n.d.	n.d.	n.d.
mg-no.	0·484	0·565	0·443	0·491	0·568	0·516	n.d.	n.d.	n.d.	n.d.	n.d.	n.d.
Rb	11	10·5	18·2	47·4	8·5	49	57·2	9·2	9·2	21·0	9·6	10·6
Sr	512	404	470	384	395	376	380	479	484	497	374	410
Y	22·5	22·2	26·1	45·5	20·6	47·3	40·2	23·4	22·7	24·6	20·6	22·4
Zr	59	37	73	162	32	169	175	51	56	69	39	44
Nb	1·7	b.d.	2·1	6·3	b.d.	7·2	7·3	1·5	2·4	2·6	2·9	1·8
Ba	389	375	519	835	309	864	672	376	375	424	361	411
Pb	7	5	6	15	b.d.	14	16	7	6	b.d.	b.d.	5
Th	b.d.	b.d.	b.d.	6	b.d.	7	10	b.d.	b.d.	b.d.	b.d.	b.d.
U	b.d.	b.d.	b.d.	b.d.	b.d.	b.d.	3	b.d.	b.d.	3	b.d.	b.d.
Sc	23	22	16	35	38	29	31	28	30	21	30	21
V	157	369	136	349	483	330	292	260	240	207	444	332
Cr	6	8	7	19	8	23	26	12	11	9	6	6
Co	25	30	17	33	35	33	33	31	30	28	36	31
Ni	b.d.	6	4	18	7	22	37	8	16	11	12	10
Cu	47	70	30	241	73	235	170	62	61	55	67	72
Zn	97	73	81	121	74	118	106	84	76	82	64	63
Ga	18	17	18	20	18	19	19	19	19	18	17	16
K (ppm)	5145	7136	8962	14521	5477	13940	12364	5560	5394	7219	6721	7634
$^{87}Sr/^{86}Sr$	n.d.	0·70442	n.d.	n.d.	n.d.	n.d.	n.d.	n.d.	n.d.	n.d.	n.d.	n.d.
IUGS class.	MKBA	MKSB	MKBA	HKSB	SB	HKSB	MKSB	MKSB	MKSB	MKSB	SB	SB

Table 2: continued

	Prehistoric lava flows of the LVF				Maar deposits of the LVF							
Sample no.:	RKR2882	TAR288	RKR126	RAR2863	RAR2864	RGP2661	RGP2662	KAR1070	KAR1071	RSN196	RWL1070	RBI5071
Locality:	Ranu Kembar E end of maar	S Parsian flow top	Ranu Kambang N end of maar	Ranu Air W crater floor	Ranu Air W crater wall	Gunung-parang E crater wall	Gunung-parang E crater wall	Kalianyar N crater wall	Kalianyar N crater wall	Ranu Segaran E crater wall	Ranu Wulung S crater wall	Ranu Bedali N crater wall
Rock type:	lava block	massive lava	lava block	scoria	lava block	lava block	lava block	lava block	lava block	lava block	lava block	lava boulder
Series:	PLF2	PLF2	PLF2									
SiO_2	48·70	52·29	50·59	45·88	52·93	52·6	50·71	52·28	50·55	50·85	50·53	51·88
TiO_2	1·010	0·771	0·942	1·019	1·561	1·742	0·983	1·655	1·02	0·957	1·963	1·786
Al_2O_3	19·22	20·25	20·93	15·50	16·45	15·91	19·76	15·72	20·55	20·13	14·99	15·58
Fe_2O_3*	11·18	10·15	10·09	13·16	12·02	12·6	10·53	13·35	9·56	8·76	15·24	13·61
MnO	0·173	0·200	0·206	0·196	0·183	0·193	0·154	0·204	0·151	0·127	0·261	0·205
MgO	4·64	3·49	3·23	10·36	3·72	3·88	3·51	3·95	2·48	2·95	4·16	3·35
CaO	9·75	8·89	9·56	12·63	7·59	7·64	8·7	7·55	9·48	9·39	8·05	7·4
Na_2O	2·75	3·21	3·48	1·76	3·12	2·93	3·24	2·96	3·14	3·12	2·67	2·96
K_2O	1·41	0·75	0·81	0·31	1·92	1·99	1·5	1·75	2·07	2·04	1·87	2·02
P_2O_5	0·228	0·259	0·216	0·090	0·41	0·474	0·251	0·397	0·562	0·392	0·521	0·446
LOI	0·81	−0·30	−0·02	−0·41	−0·42	−0·24	0·26	0·12	0·68	1·02	−0·2	0·26
Total	99·87	99·95	100·02	100·50	99·48	99·72	99·6	99·94	100·24	99·74	100·05	99·5
FeOt	n.d.	n.d.	n.d.	n.d.	n.d.	n.d.	n.d.	n.d.	n.d.	n.d.	n.d.	n.d.
Fe_2O_3t	n.d.	n.d.	n.d.	n.d.	n.d.	n.d.	n.d.	n.d.	n.d.	n.d.	n.d.	n.d.
mg-no.	n.d.	n.d.	n.d.	n.d.	n.d.	n.d.	n.d.	n.d.	n.d.	n.d.	n.d.	n.d.
Rb	27·8	10·7	11·8	3·2	65·1	n.d.	33·8	n.d.	58·0	54·3	71·4	65·4
Sr	579	591	512	289	366	n.d.	535	n.d.	626	626	333	324
Y	21·5	24·4	26·5	15·9	42·9	n.d.	21·1	n.d.	30·1	23·6	55·8	49·5
Zr	65	69	60	21	186	n.d.	63	n.d.	136	97	221	197
Nb	3·4	3·2	3·3	1·6	6·8	n.d.	4·8	n.d.	11·1	7·4	9·4	8·0
Ba	417	433	414	195	1007	n.d.	469	n.d.	646	670	865	988
Pb	b.d.	b.d.	b.d.	b.d.	15	n.d.	6	n.d.	9	9	18	16
Th	5	b.d.	b.d.	b.d.	9	n.d.	5	n.d.	13	7	10	9
U	b.d.	b.d.	b.d.	b.d.	b.d.	n.d.	b.d.	n.d.	4	b.d.	6	3
Sc	24	23	21	62	26	n.d.	26	n.d.	23	24	41	32
V	306	148	173	439	286	n.d.	296	n.d.	198	215	407	352
Cr	18	6	4	100	13	n.d.	8	n.d.	10	25	19	10
Co	33	24	21	56	34	n.d.	29	n.d.	24	22	32	32
Ni	21	13	15	46	18	n.d.	13	n.d.	24	34	28	28
Cu	154	67	71	69	306	n.d.	114	n.d.	243	155	241	151
Zn	74	79	73	79	101	n.d.	93	n.d.	76	70	131	116
Ga	18	20	18	16	18	n.d.	20	n.d.	18	18	21	20
K (ppm)	11700	6223	6721	2572	15932	16513	12447	14521	17177	16928	15517	16762
$^{87}Sr/^{86}Sr$	n.d.	n.d.	n.d.	n.d.	n.d.	n.d.	n.d.	n.d.	n.d.	n.d.	n.d.	n.d.
IUGS class.	HKSB	MKBA	MKSB	SB	HKBA	HKBA	HKBA	HKBA	PT	PT	HKSB	HKBA

	Other East Javanese volcano data						
Volcano:	Semeru						Bromo
Sample no.:	SEM1607	SEM1409	SEM41a	SEM41b	SEM41c	SEM41d	BRO1
Locality:	Feb. 94 pf Curah Kobokan	Semeru summit	1941–1942 flow W G. Sawur VO	1941–1942 flow flow top	1941–1942 flow flow top	1941–1942 flow flow edge	G. Bromo Tengger Caldera
Rock type:	1994 lava dome	lava bomb	lava block	lava block	lava block	lava block	March 95 bomb
SiO_2	56·31	56·52	58·37	57·25	57·42	58·59	56·36
TiO_2	0·714	0·704	0·666	0·689	0·692	0·668	1·012
Al_2O_3	19·57	19·85	18·34	19·45	19·51	18·36	17·66
Fe_2O_3*	7·66	7·63	8·22	7·42	7·44	8·21	8·84
MnO	0·176	0·171	0·232	0·173	0·168	0·231	0·157
MgO	2·28	2·24	2·37	2·10	2·12	2·41	2·36
CaO	7·98	7·97	6·88	7·50	7·51	6·88	6·92
Na_2O	3·57	3·55	3·75	3·75	3·76	3·74	3·26
K_2O	1·23	1·22	1·14	1·29	1·31	1·14	2·81
P_2O_5	0·176	0·178	0·198	0·184	0·185	0·193	0·445
LOI	0·1	−0·10	−0·34	−0·07	−0·04	−0·19	−0·17
Total	99·77	99·93	99·82	99·73	100·08	100·22	99·65
FeOt	n.d.	n.d.	n.d.	n.d.	n.d.	n.d.	n.d.
Fe_2O_3t	n.d.	n.d.	n.d.	n.d.	n.d.	n.d.	n.d.
mg-no.	n.d.	n.d.	n.d.	n.d.	n.d.	n.d.	n.d.
Rb	28·1	28·1	23·5	28·4	28·4	23·8	105
Sr	416	417	442	412	405	446	396
Y	23·7	23·8	27·1	25·0	25·6	27·9	48·3
Zr	90	93	94	99	97	94	239
Nb	2·6	3·0	3·7	3·5	3·2	2·8	9·2
Ba	544	541	571	558	540	522	860
Pb	10	10	7	10	10	9	18
Th	4	b.d.	5	b.d.	5	b.d.	17
U	b.d.	b.d.	b.d.	b.d.	b.d.	b.d.	3
Sc	15	15	14	13	13	11	22
V	112	104	52	95	92	46	108
Cr	b.d.	4	5	5	4	5	9
Co	15	14	12	14	16	14	16
Ni	3	9	9	12	9	7	5
Cu	56	51	13	61	61	20	127
Zn	83	78	95	82	83	97	89
Ga	20	20	17	20	19	17	18
K (ppm)	10206	10115	9451	10696	10870	9435	23317
$^{87}Sr/^{86}Sr$	n.d.	n.d.	n.d.	n.d.	n.d.	n.d.	n.d.
IUGS class.	MKBA	MKBA	MKA	MKA	MKA	MKA	L

All analyses by XRF, except Sr isotopic ratios by IDMS. Oxides reported in wt %, trace elements in ppm. Fe_2O_3*, total Fe as Fe_2O_3; FeOt and Fe_2O_3t, oxides determined by titration for selected samples; n.d., not determined; LOI, loss on ignition. Trace element detection limits (ppm) are: 2 (Rb, Sr, Y, Zr, Co), 1·5 (Nb), 12 (Ba), 5 (Pb, Sc, V), 4 (Th, Cr), 3 (U, Ni, Cu, Zn, Ga); b.d., below detection limits. IUGS classifications, based on the total alkali–silica (TAS) diagram, are: picrobasalt (PB), subalkali basalt (SB), low-K subalkali basalt (LKSB), medium-K subalkali basalt (MKSB), high-K subalkali basalt (HKSB), medium-K basaltic andesite (MKBA), high-K basaltic andesite (HKBA), low-K andesite (LKA), medium-K andesite (MKA), high-K dacite (HKD), basanite (BS), potassic trachybasalt (PT), shoshonite (SH), latite (L).

Table 3: Modal proportions (vol. %, vesicle-free) of glomerocryst (Gl), phenocryst (Ph) and groundmass (Gm) phases in selected LVF rocks (point-counted using 700-1000 points per sample)

Sample	Plag %				Olivine %			Pyroxene %			Oxides %	Glass %	Others %	Crystals %
	Gl	Ph	Gm	Total	Ph	Gm	Total	Ph	Gm	Total				
LAM18982	9·3	22·2	38·5	70·0	3·1	5·0	8·1	8·1	0	8·1	11·9	0	1·9	100
LAM18832	9·9	17·6	27·8	55·4	2·8	3·9	6·6	4·7	0	4·7	13·8	13·8	2·5	86·2
LAM18641	20·0	15·8	32·7	68·5	2·0	2·4	4·5	11·5	0	11·5	9·3	5·8	0·2	94·2
LAM1070	24·5	19·4	22·5	66·4	6·0	0·9	6·9	2·1	10·2	12·3	8·1	6·3	0	93·7
LAM1261	20·2	11·3	32·0	63·5	6·5	0·8	7·3	3·7	9·9	13·6	7·3	8·4	0	91·6
LAM1562	22·9	17·4	22·9	63·1	5·3	0·8	6·1	1·4	10·6	12·1	6·8	11·9	0	88·1
LAM1564	23·9	12·6	26·1	62·5	3·9	3·7	7·7	2·2	7·0	9·2	5·8	15·3	0	84·7
LAM2962	17·1	14·4	27·1	58·5	4·4	1·9	6·3	5·8	8·1	14·0	9·4	11·7	0	88·3
LAM7070	23·1	18·0	25·0	66·1	8·5	2·5	11·0	0·6	10·6	11·2	9·8	2·0	0	98·0
LAM1762	25·4	21·3	22·4	69·1	5·0	0·5	5·5	3·5	13·8	17·3	7·8	0·3	0	99·7
ALA1161	0	8·6	28·0	36·6	1·1	3·6	4·7	4·8	11·5	16·3	7·7	34·6	0	65·4
GCK2960	14·1	22·4	25·5	61·9	6·7	0·7	7·5	6·5	14·4	20·9	8·7	1·1	0	98·9
GKL256	9·7	21·5	23·8	55·1	8·1	2·4	10·6	8·0	12·1	20·1	13·7	0·4	0	99·6

have controlled their distribution in the chamber and biased their occurrence to earlier-erupted flows.

Cinder or spatter cones

Samples from the LVF cinder or spatter cones display a wide range of petrographic features. Following Carn (2000), the cones are subdivided morphologically into a young series (centuries old) and an old series (millennia old; Fig. 2). The former is referred to as the kerucut volkanik muda (KVM) series and the latter as the kerucut volkanik tua (KVT) series. Cinder cones observed within maars belong to the KVM series. The KVT cones are generally situated in the western part of the LVF (Fig. 2). The modal mineralogy of three KVM samples is given in Table 3.

The KVM lavas contain phenocrysts of *Plag*, *Cpx*, Fe–Ti oxides and *Ol*. Very rare crystals of oxy-hornblende are also present in two scoria samples (ALA1161 and GCK2961). Many of the KVM cones are spatter ramparts associated with flank lava flows (Fig. 2), and samples from these flows (e.g. GCK2960, GKL256) are similar in appearance and modal mineralogy to the historical lavas (Table 3). Large *Cpx* phenocrysts (up to ~7 mm long, often euhedral) are common in the KVM lava flows, typically with inclusions of Fe–Ti oxides, often concentrated at crystal rims (as observed in the historical lavas). Some *Cpx* shows resorption features (e.g. embayments, eroded rims, sieve texture) and exsolution lamellae are common. *Ol* phenocrysts (up to 6 mm long) and microphenocrysts (<1·5 mm long) are usually embayed and occasionally skeletal. *Plag* is abundant and sometimes occurs as glomerocrysts, but less commonly than observed in the historical samples (Table 3), and disequilibrium textures in *Plag* are also present, but less widespread in the KVM samples. *Plag* phenocrysts are typically a maximum of ~1·5 mm in length. Fe–Ti oxides are abundant, particularly in the groundmass; phenocrysts are up to 2 mm in size. Cumulate clots of *Plag*, *Cpx* and Fe–Ti oxides, similar to those discerned in the historical lavas, are also evident in the KVM lava flow samples. There is a general trend of decreasing phenocryst dimensions with distance from the central (LTT) edifice.

Other KVM samples are basaltic scoriae or small bombs, and hence contain more groundmass glass than the associated lava flows (e.g. ALA1161, Table 3). The scoriae have the same mineralogy as the lavas (with the exception of the two samples that contain minor oxy-hornblende), although phenocrysts are generally smaller in the former; typically <1 mm with rare *Cpx* up to ~5 mm and *Plag* up to 3–4 mm in length. Other textural features are similar, such as the mantling of *Cpx* phenocrysts by Fe–Ti oxide inclusions, the presence of cumulate nodules (maximum 5 mm diameter; largely *Cpx* and Fe–Ti oxides), and some resorptional features in *Ol*, *Cpx* and *Plag* crystals. Glomerocrysts are typically absent or rare and disequilibrium textures are less common than in the historical samples.

KVT samples are petrographically diverse but some spatial patterns can be discerned. Cones in the western

LVF, west of the town of Klakah (Fig. 2), are particularly distinct and represent some of the oldest vents in the complex (Carn, 2000). Samples from these cones are generally glassy and contain *Plag*, *Ol* and minor *Cpx* in order of decreasing abundance. *Plag* typically exists as microlites (normally aligned) or microphenocrysts, often zoned and occasionally showing disequilibrium textures in larger crystals, which may have fresh mantles. Glomerocrysts of *Plag* up to 3–4 mm in diameter are also observed in some samples, and individual phenocrysts range up to ~3 mm in length. *Ol* occurs as microphenocrysts (up to ~1·5 mm in size), which are frequently embayed or skeletal. *Cpx* appears rare in these samples and is generally restricted to the groundmass.

Other KVT samples form localized groups with distinctive petrography, although they are generally akin to the KVM lavas. Textural similarities are observed between samples from collinear vents (e.g. GMI15072 and GKN3060; both highly *Plag*-phyric).

Prehistoric lavas

Prehistoric lava flows (PLFs) are distributed throughout the LVF although they are rarely well exposed. Samples from outlying flows (PLF1; e.g. TAR1361, KAP2062, RBI1162; Fig. 2) are typically *Plag*-phyric with a glassy matrix. *Cpx* and *Ol* are present as microphenocrysts (~1 mm) although *Ol* is often unstable. *Plag* crystals are usually flow-aligned and show rare disequilibrium textures. Some clots (~1 mm diameter) of *Cpx*, Fe–Ti oxides and *Plag* are also present, and the groundmass is often rich in Fe–Ti oxides.

The other PLF samples form two distinct groups. One set (PLF2) crops out around much of the flank region of the LTT edifice, usually in the walls of maar craters as thick flows (e.g. RWG116, RJN278, RAG1962, RLG1262; Figs 2 and 3); these lavas are highly porphyritic, containing phenocrysts of *Ol*, *Plag* and *Cpx* in a coarse groundmass (same mineralogy, plus Fe–Ti oxides). *Ol* is typically anhedral and unstable (skeletal in places), occurring as microphenocrysts and phenocrysts up to ~3 mm in length and occasionally in nodules (with variable amounts of Fe–Ti oxides, *Cpx* and *Plag*) several millimetres in diameter. *Plag* often occurs as glomerocrysts (3–4 mm in size), and frequently displays sieve-texture and fine-scale compositional zoning, the latter sometimes mantling the former. *Cpx* phenocrysts (3–6 mm) and glomerocrysts (up to 1 cm long) are less abundant, sometimes euhedral, but generally unstable. Some contain inclusions of *Ol*, *Plag* and Fe–Ti oxides (concentrated at the edges of the host crystal).

The other group (PLF3) crops out at a slightly higher stratigraphic level in flows with seldom pristine morphologies, largely on the flanks of Lamongan (e.g. LAO306, LAO1207, TAR2760; Figs 2 and 3). Their petrography exhibits many similarities with the historical samples from Lamongan.

MINERALOGY

The major phenocryst phases in LVF lavas are *Ol* (Fig. 4), *Cpx* (Fig. 4), *Plag* (Fig. 5) and Fe–Ti oxides. Representative mineral analyses are presented in Tables 4–6, and a summary of observed mineral compositions is given in Table 7. The majority of Fe–Ti oxide crystals analysed fall on the magnetite–ulvöspinel solid solution (titanomagnetite), with TiO_2 contents as high as 17 wt % but typically around 7–10 wt %.

Olivine

Forsterite (*Fo*) contents of *Ol* phenocrysts and microphenocrysts in LVF lavas range from Fo_{29} to Fo_{79}, with considerable variation often observed on the scale of individual samples (Table 7). This variation is generally greater in the historical lavas. Many crystals display normal zoning (Table 4). The more *Fo*-rich crystals are generally found in cinder cone samples, and *Fo* contents are typically highest in glomerocrysts and crystals found in cumulate clots or nodules, with microphenocrysts typically more iron rich. Disequilibrium textures in *Ol* are seen in a range of compositions (Table 4). CaO contents rarely exceed ~0·3 wt %, which is a typical value for basaltic olivines (Jurewicz & Watson, 1988) and higher than that found in mantle olivines (<0·1 wt %; e.g. Foden, 1983).

There is widespread evidence for *Ol* accumulation in LVF lavas. *Ol* phenocrysts and microphenocrysts are typically not in equilibrium with their host rock, with *Fo* contents generally being too low for their respective bulk-rock *mg*-number; this is particularly evident in the historical lavas and PLFs (Fig. 6). This may be due to elevation of the measured Fe_2O_3/FeO (wt %) ratio by post-eruption alteration and oxidation, which would result in artificially high *mg*-numbers. However, most lavas were not visibly altered, with the exception of some PLF2 samples that show iddingsite rims on *Ol* phenocrysts (e.g. RAG1962), which may explain the more extensive disequilibrium in these samples (Fig. 6). Assuming an Fe_2O_3/FeO ratio of 0·2 still places the majority of historical samples and PLFs in disequilibrium, although the cinder cones (largely KVM) plot close to the high-pressure equilibrium field (Fig. 6). Cinder cone *Ol* also shows the narrowest range of *Fo* contents, particularly sample ALA1161 (KVM), whereas the PLF2 samples (RWG116, RAG1962; Fig. 6) show the clearest evidence for *Ol* accumulation. Mean *Fo* contents in *Ol* are 63% (historical lavas), 74% (cinder cones) and 62% (PLFs).

Table 4: Representative olivine analyses

	Cinder cones							PLFs			Historic lava flows				
Sample:	GCK1071		GKL-256	GGI2661		GOO13071		LAO296		RA-1	LAM-1561	LAM18981		LAM1070	
Xtal:	Phxt	Phxt	Mphxt	Phxt	Phxt	Phxt	Phxt	Phxt	Phxt	Glxt	Mphxt	Mphxt	Mphxt	Mphxt	Mphxt
Core/rim:	Core	Rim	Core	Core	Rim	Core	Rim	Core	Rim	Core	Core	Core	Rim	Core	Rim
Texture:			Res			Emb	Emb	St	Res					St	
SiO_2	38·84	38·72	38·42	38·55	37·86	36·59	36·80	37·88	36·55	38·81	35·81	37·41	36·34	35·75	36·00
FeO	18·95	20·60	22·45	20·97	23·70	31·14	29·41	25·34	32·24	21·02	35·98	25·65	31·27	35·74	35·30
MnO	0·36	0·36	0·46	0·29	0·51	0·56	0·53	0·53	0·91	0·39	0·92	0·61	0·69	0·88	0·80
MgO	41·08	39·90	38·43	39·92	36·98	30·32	31·85	36·09	29·85	39·43	26·81	35·29	30·74	27·42	27·80
CaO	0·22	0·20	0·23	0·23	0·30	0·28	0·29	0·26	0·29	0·14	0·20	0·26	0·29	0·24	0·23
Total	99·46	99·78	99·98	99·96	99·35	98·88	98·89	100·1	99·86	99·80	99·72	99·21	99·32	100·04	100·13
Fo	79·4	77·5	75·3	77·2	73·5	63·4	65·9	71·7	62·3	77·0	57·1	71·0	63·7	57·8	58·4
Fa	20·6	22·5	24·7	22·8	26·5	36·6	34·1	28·3	37·7	23·0	42·9	29·0	36·3	42·2	41·6

Oxides in wt %. Glxt, Phxt, Mphxt, glomerocryst, phenocryst, microphenocryst, respectively. Textures: Res, resorbed; Emb, embayed; St, sieve texture. Fo, Fa, molar percentages of forsterite and fayalite, respectively.

Table 5: Representative pyroxene analyses

	Cinder cones					PLFs		Historic lava flows			
Sample:	GCK1071	GKL256		GGI2661	ALA1161	RA-1		LAM1561		LAM18981	LAM2961
Xtal:	Glxt	Mphxt	Mphxt	Mphxt	Mphxt	Phxt	Phxt	Glxt	Glxt	Phxt	Mphxt
Core/rim:	Core	Core	Rim	Core	Core	Core	Rim	Core	Rim	Core	Core
Texture:								St			
SiO_2	46·96	47·66	48·14	45·61	48·96	48·62	48·10	51·53	51·48	50·48	52·37
TiO_2	1·12	1·27	1·28	1·36	0·99	0·63	0·94	0·37	0·46	0·64	0·32
Al_2O_3	7·14	6·98	5·47	8·63	4·86	6·70	7·00	2·83	2·34	2·93	3·23
Cr_2O_3	0·02	0·06	0·09	0·06	0·07	0·47	0·26	0·08	0·09	0·07	0·09
FeO	7·90	7·61	9·62	8·45	7·77	6·40	6·72	20·46	12·71	9·18	22·45
MnO	0·11	0·14	0·28	0·10	0·13	0·15	0·09	0·73	0·62	0·28	0·84
MgO	12·40	12·77	12·28	12·16	14·03	13·95	13·31	22·24	15·07	14·15	14·06
CaO	23·46	23·16	22·30	22·96	22·87	23·02	22·76	1·78	16·96	21·02	5·44
Na_2O	0·39	0·35	0·41	0·45	0·35	0·26	0·31	0·13	0·48	0·42	0·81
Total	99·51	100·00	99·87	99·79	100·03	100·21	99·49	100·2	100·2	99·16	99·61
Mg	36·8	37·9	36·4	36·4	40·3	40·9	39·8	63·5	43·8	41·1	46·0
Fe	13·2	12·7	16·0	14·2	12·5	10·5	11·3	32·8	20·7	15·0	41·2
Ca	50·0	49·4	47·5	49·4	47·2	48·5	48·9	3·7	35·4	43·9	12·8

Oxides in wt %. Abbreviations as in Table 4. Mg, Fe, Ca, molar percentages of enstatite, ferrosilite and wollastonite, respectively.

Table 6: Representative plagioclase analyses

	Cinder cones										PLFs		Historic lava flows							
Sample:	GKL256		GGI2661		GOO13071		ALA1161		GKK1107		RA-1		LAO296		LAM1561		LAM1763		LAM18981	
Xtal:	Phxt	Phxt	Mphxt	Mphxt	Phxt	Phxt	Mphxt	Mphxt	Glxt	Glxt	Phxt	Phxt	Glxt	Glxt	Phxt	Phxt	Phxt	Phxt	Phxt	Phxt
Core/rim:	Core	Rim	Core	Rim	Core	Rim	Core	Rim	Core	Rim	Core	Rim	Core	Rim	Core	Rim	Core	Rim	Core	Rim
Texture:	Res	Res			St	St							St		St	St	St	St		
SiO_2	44·31	50·41	44·65	52·85	52·51	51·11	46·44	46·06	44·01	45·94	44·48	53·61	44·79	48·95	48·19	65·82	45·66	58·26	44·54	51·98
Al_2O_3	34·93	30·47	34·38	28·65	28·97	29·83	33·14	33·00	34·90	32·92	34·90	28·41	34·37	31·36	31·93	16·99	33·38	25·08	34·80	29·59
FeO	0·54	0·86	0·50	0·95	0·65	0·86	0·80	0·69	0·49	0·97	0·69	0·83	0·52	0·90	0·52	3·58	0·76	0·85	0·52	0·87
CaO	19·23	14·31	19·02	12·43	12·82	14·08	17·77	17·62	19·39	17·52	19·12	11·87	18·81	15·37	16·00	4·19	17·87	8·24	19·05	13·42
Na_2O	0·68	3·39	0·91	4·71	4·13	3·63	1·54	1·67	0·55	1·62	0·70	4·50	0·95	2·83	2·58	5·06	1·54	6·81	0·61	4·03
K_2O	0·03	0·20	0·06	0·27	0·40	0·31	0·09	0·05	0·02	0·07	0·01	0·39	0·04	0·16	0·08	2·15	0·01	0·58	0·01	0·19
Total	99·71	99·65	99·53	99·87	99·48	99·82	99·79	99·09	99·36	99·03	99·90	99·61	99·48	99·57	99·30	97·79	99·21	99·81	99·52	100·1
An	93·8	69·2	91·7	58·4	61·7	67·0	86·0	85·1	95·0	85·3	93·7	58·0	91·4	74·3	77·1	26·3	86·5	38·8	94·5	64·1
Ab	6·0	29·7	8·0	40·1	36·0	31·3	13·5	14·6	4·9	14·3	6·2	39·8	8·4	24·8	22·5	57·5	13·5	58·0	5·5	34·8
Or	0·2	1·2	0·4	1·5	2·3	1·8	0·5	0·3	0·1	0·4	0·1	2·3	0·2	0·9	0·5	16·1	0·1	3·2	0·1	1·1

Oxides in wt %. Abbreviations as in Table 4. An, Ab, Or, molar percentages of anorthite, albite and orthoclase, respectively.

Table 7: Summary of mineral compositions in LVF samples

Sample	Olivine (Fo)	*n*	Zoning	Pyroxene (En, Fs, Wo)	*n*	Zoning	Plag (An)	*n*	Zoning
Historical lava flows									
LAM18981	74–29	22	N	36–42, 12–19, 43–48	24	N	95–60	67	N, R, O
LAM18831	69–46	17	N	—	—	—	91–50	45	N, O
LAM18642	65–44	26	N	38–54, 19–37, 9–43	20	N	94–34	50	N, R, O
LAM1070	65–52	26	N	39–55, 23–35, 10–38	13	N	92–40	64	N, O
LAM2961	66–41	23	N	39–46, 23–41, 13–38	11	N	90–26	66	N
LAM1762	59–46	6	—	—	—	—	86–52	24	N, O
LAM1207	69–55	17	—	37–42, 34–35, 24–28	2	—	89–43	40	N, O
LAM1563	64–42	24	N	15–43, 17–45, 40–46	16	—	93–24	56	N
LAM1561	63–48	20	—	34–65, 13–32, 3–52	21	—	87–26	58	N, O
LAM1761	72–36	37	—	20–43, 17–29, 41–51	40	—	93–24	96	N, R, O
LAM6071	68–59	9	—	38–42, 16–57, 5–41	9	—	89–23	65	N, O
LAM1763	73–36	29	—	38–43, 14–21, 41–42	29	N	91–28	66	N
LAM7070	68–37	29	N	36–42, 19–25, 39	13	N	88–29	58	N, R, O
Cinder cones									
GKK1107	78–64	23	—	24–41, 12–31, 45–47	4	—	96–59	41	N
GCK1071	79–40	12	N	37–41, 13–15, 48–50	4	—	94–31	13	—
ALA116	78–74	11	—	10–47, 21–56, 32–34	33	N	96–71	26	N
GOO13071	70–60	31	—	50, 25, 25	1	—	79–39	87	N
GGI2661	77–61	44	—	34–41, 12–15, 47–51	31	N	93–58	46	N
GKL256	77–32	23	N	20–39, 13–16, 47–65	49	N, R	95–29	72	N, O
Prehistoric lava flows									
RWG116	68–51	39	N	38–43, 17–21, 36–44	10	—	93–28	43	N, O
RAG1962	78–58	22	N	39–42, 11–15, 43–49	16	—	95–43	52	N, O
LAO296	72–47	24	N	34–41, 16–20, 43–46	13	N, R	94–31	61	N, O

n, number of analyses. Zoning: N, normal; R, reverse; O, oscillatory.

Pyroxene

The vast majority of pyroxenes are typical augites (Fig. 4), with minor low-Ca pyroxene observed only in the more evolved historical lavas, and rare ferroaugite. Where present, low-Ca pyroxene is occasionally mantled by *Cpx* and often unstable. As mentioned above, inclusions of *Mag* are very common towards the rims of pyroxene phenocrysts. This may be a reaction texture resulting from the breakdown of unstable Fe-rich pyroxene, or an oxidation effect. Pyroxenes can contain high concentrations of structurally bound OH (up to 110 ppm H_2O), particularly mantle pyroxenes (e.g. Skogby, 1994). Such OH may provide fuel for oxidation–dehydroxylation reactions that occur during the formation of oxy-hornblende and convert Fe^{2+} to Fe^{3+}. Phenocryst rims and groundmass crystals are typically more Fe rich. CaO contents in excess of 23 wt % (salite) are not uncommon in samples from cinder cones and PLFs (Table 5). Chromian pyroxene is absent, with Cr_2O_3 typically <0·1 wt %.

Pyroxenes from cinder cone and PLF samples are distinguished by their high Al contents, often in excess of 5 wt %, and also by high TiO_2 ($\sim$1 wt % or more; Table 5). Al_2O_3 concentrations in clinopyroxene from subcontinental and suboceanic peridotites range from 2 to 8 wt %, with decreasing Al associated with increasing proportions of coexisting melt (Seyler & Bonatti, 1994). Similar augites and Ti-rich aluminous salites to those found in the LVF have been reported in alkaline (potassic) basalts from Ringgit–Beser, an extinct volcanic complex situated on the north coast of East Java (Fig. 1; Edwards *et al.*, 1994), and in calc-alkaline basalts from behind the

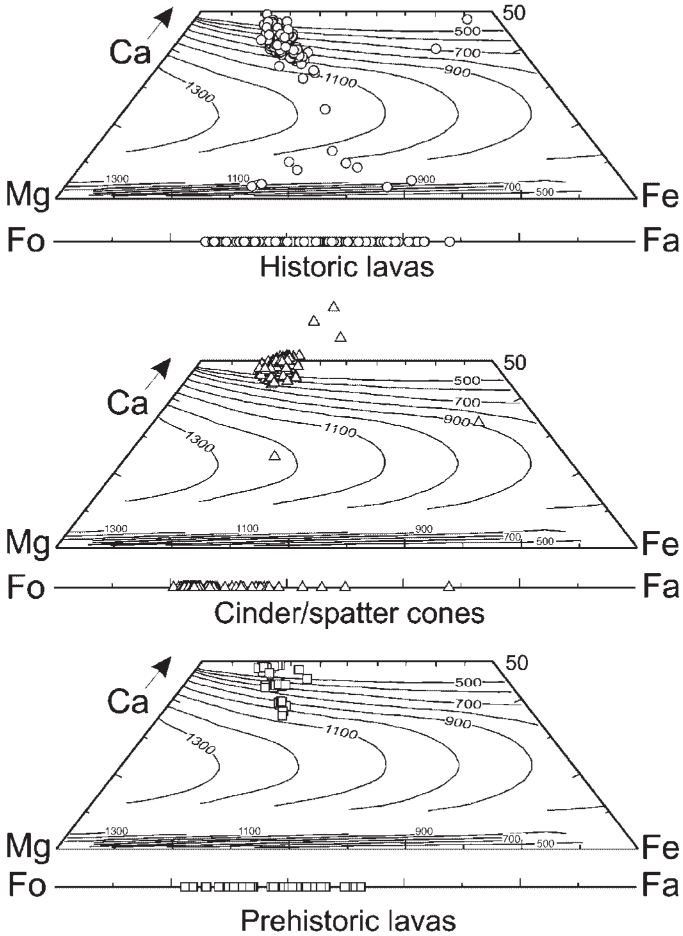

Fig. 4. Pyroxene and olivine phenocryst compositions, plotted on the pyroxene quadrilateral and *Fo–Fa* tie-line respectively, for LVF historical lavas, cinder or spatter cones and prehistoric lavas. Tie-lines in the pyroxene quadrilateral join coexisting CPX and OPX phenocrysts at 5 kbar, based on the thermometry of Lindsley (1983). Ticks are in increments of 10%.

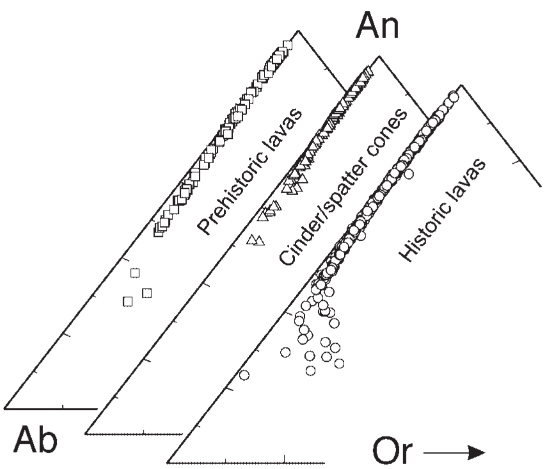

Fig. 5. Plagioclase phenocryst compositions plotted on the *An–Ab–Or* ternary, for LVF historical lavas, cinder or spatter cones and prehistoric lavas. Ticks are in 10% increments.

volcanic front along the Sangihe arc north of Sulawesi (Morrice & Gill, 1986).

Plagioclase

Plag exhibits a wide compositional range in many samples, with a maximum anorthite (*An*) content of ~96 mol % (Table 7; Fig. 5). The more *An*-rich compositions are found in glomerocrysts and as phenocryst cores (Table 6), and are more common in cinder cone samples.

Highly calcic plagioclase is common in high-Al arc basalts, with *An* content dependent upon the H_2O content, crystallization pressure, Al_2O_3 content and CaO/Na_2O value of the melt (e.g. Panjasawatwong *et al.*, 1995). Melt CaO/Na_2O exerts the strongest control on plagioclase *An* content, with values of $CaO/Na_2O > 8$ required to produce highly calcic (An_{95}) plagioclase as observed in the LVF samples. The highest CaO/Na_2O ratios in the LVF suite (~6–7) occur in the KVM lavas from the

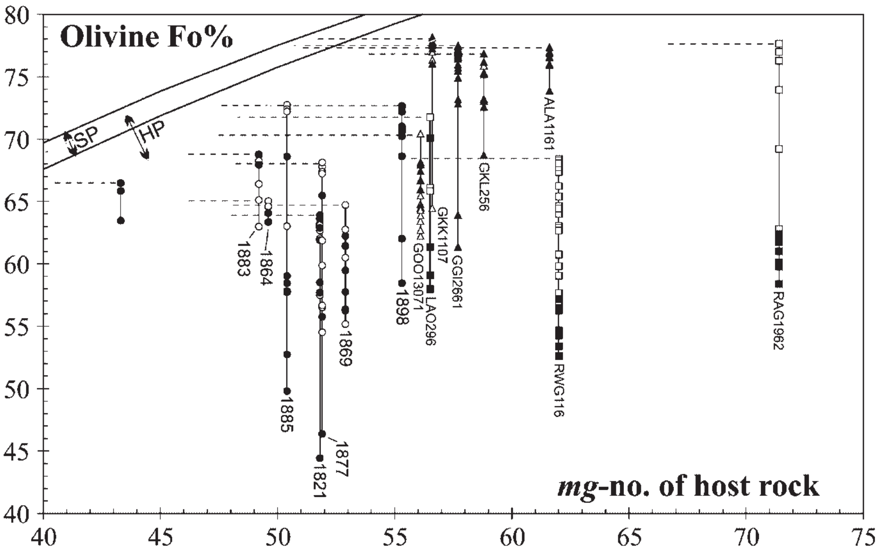

Fig. 6. Forsterite (*Fo*) contents of olivines vs *mg*-number [100Mg/(Mg + Fe^{2+})] of host basalts. *mg*-number is calculated using the Fe-oxide ratios determined by titration (Table 2). Data shown are for historical lavas (●, ○), cinder cones (△, ▲) and PLFs (□, ■); symbols represent phenocrysts and microphenocrysts, respectively. Historical lavas are labelled with eruption dates (where known); cinder cones and PLFs are labelled with sample names. Dotted lines show where the data would plot if *mg*-numbers were recalculated assuming Fe_2O_3/FeO = 0·2. The shallow-pressure (SP) and high-pressure (HP) equilibrium fields for basaltic magma (Roeder & Emslie, 1970; Ulmer, 1989) are indicated.

northern and western flanks of LTT (Fig. 2), which also contain *An*-rich *Plag* (Table 7), but these are probably not true liquid compositions. High values (CaO/Na_2O ~7) also occur in the PLF2 samples, although these are highly phyric.

Disequilibrium textures (embayed crystals, sieve texture, etc.) are common in *Plag* (particularly in the historical lavas and the PLF2–PLF3 samples) but are not restricted to a particular compositional range. Zoning of several types (normal, reverse, oscillatory) is prevalent in *Plag*, especially in the historical lavas (Table 7). Sieve-textured or cellular *Plag* can form through resorption (e.g. as a result of decreasing *P*, increasing P_{H_2O}, or mixing with hotter magma) or rapid crystal growth under vapour-saturated conditions or after mixing with cooler magma (e.g. Tsuchiyama, 1985; Morrice & Gill, 1986). These processes can be distinguished using textural evidence, because resorption leads to cellular zones with diffuse inner boundaries, whereas rapid growth results in zones with sharp borders, often associated with oscillatory zoning. The latter appear to dominate in the LVF lavas, although the cellular cores of *Plag* are often more diffuse.

Amphibole

The occurrence of amphibole in the LVF lavas is restricted to rare phenocrysts of oxy-hornblende in two KVM samples. These crystals were not analysed by electron microprobe. They have narrow rims of fine-grained oxides, with dark brown pleochroic interiors. The relatively high oxide content of some samples may indicate widespread oxidation and breakdown of amphibole in LVF magmas, which is only rarely preserved.

GEOCHEMISTRY

Overview

Whole-rock major and trace element XRF data for the LVF suite are reported in Table 2. In Fig. 7, the LVF data are compared with existing analyses from other active and extinct Indonesian volcanoes. The least evolved LVF basalts (~43 wt % SiO_2) represent some of the most SiO_2-poor lavas reported from the archipelago to date, considerably lower than the mean SiO_2 of 55·5 wt %. Although many of the LVF lavas have higher MgO contents than the relatively low Indonesian average of 4·5 wt % (calculated from the data in Fig. 7b), they also have rather low MgO at a given value of SiO_2 in comparison with other Indonesian volcanoes. K_2O contents in LVF samples are lower than the mean of 2·5 wt % for the data in Fig. 7a.

Variations in K_2O content broadly divide the LVF suite into two series, a medium-K series and a high-K calc-alkaline series (Fig. 8a). In Fig. 8, the LVF lavas are plotted along with data from Semeru and Bromo (Fig. 1) and from Iliboleng and Lewotolo, which lie east of Flores and north of the arc–continent collision zone (Fig. 1). The bulk of the LVF samples, including the historical lavas, most of the KVM series and the PLF2 and PLF3

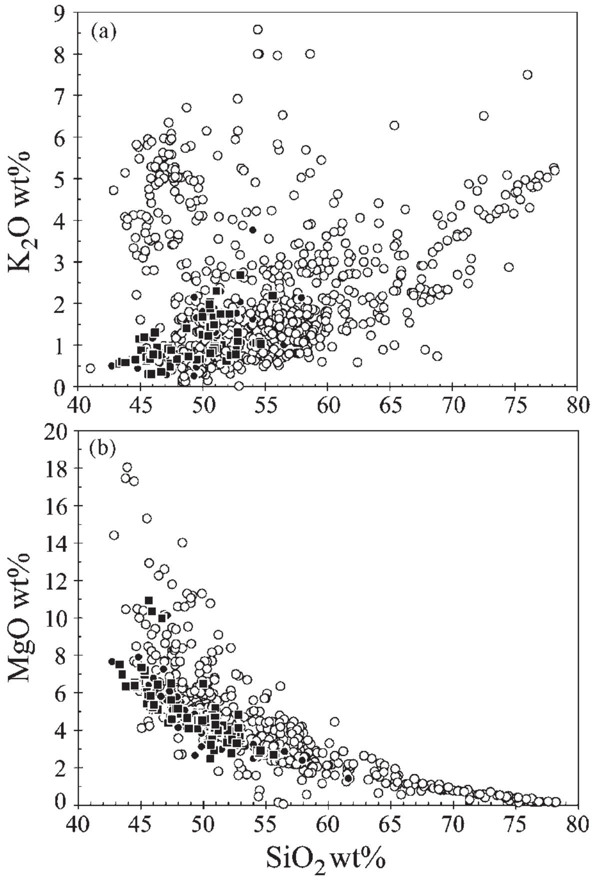

Fig. 7. (a) K_2O vs SiO_2 data for LVF lavas from this study (■) and from Mulyana (1989) (●), plotted with 678 existing analyses (○) from active and extinct volcanoes of Java, Sumatra, the Lesser Sunda Islands, the Banda Arc, Sulawesi, Maluku, Sangihe and Halmahera. Data sources: Whitford (1975), Nicholls & Whitford (1976, 1983), Whitford *et al.* (1979, 1981), Foden & Varne (1980), Hutchison (1982), Foden (1983), Self *et al.* (1984), Wheller & Varne (1986), Camus *et al.* (1987), Wheller *et al.* (1987), Stolz *et al.* (1988, 1990), Van Bergen *et al.* (1989), Varekamp *et al.* (1989), Vukadinovic & Nicholls (1989), Leterrier *et al.* (1990), Wahyudin (1991), Gerbe *et al.* (1992), Edwards *et al.* (1993, 1994), Van Gerven & Pichler (1995), Vukadinovic (1995), Vukadinovic & Sutawidjaja (1995), Mandeville *et al.* (1996), Self & King (1996) and Chesner (1998). (b) MgO vs SiO_2 for LVF lavas from this study and Mulyana (1989), plotted with 374 existing analyses from other Indonesian volcanoes. Symbols and data sources as in (a).

samples, fall in the medium-K field and form an array that continues to higher SiO_2 through the Semeru lavas. Crystal accumulation in the PLF2 series may have displaced them towards transitional tholeiitic compositions (Fig. 8a). The KVT series, PLF1 samples and the maar deposits generally lie in the high-K field, along with the rocks from the Bromo–Tengger complex and the eastern Sunda arc (Iliboleng, Lewotolo). Similar patterns emerge from a total alkali–silica plot (Fig. 8b), wherein the majority of LVF lavas are classified as typical basalts with subordinate picrobasalts (KVM series), basaltic andesites (including the oldest historical flows), trachybasalts and basaltic trachyandesites.

As is commonly observed in subduction-related volcanic rock classification (e.g. Vukadinovic & Sutawidjaja, 1995), the use of different parameters to categorize the LVF lavas gives slightly contradictory results. On an AFM diagram (Fig. 9) the LVF samples straddle the tholeiitic–calc-alkaline boundary with a definite tholeiitic tendency, showing marked Fe enrichment with respect to the Semeru and Bromo–Tengger lavas, particularly at intermediate compositions. This is contrary to the K_2O plot (Fig. 8a), but as Vukadinovic & Sutawidjaja (1995) pointed out, the two methods of discrimination probably relate to mutually exclusive aspects of the lava suite, namely its source (K_2O) and its crystallization history (AFM). The LVF samples are thus relatively and variably K rich (probably inherited from the source) and also show Fe enrichment (probably related to magma chamber processes).

Major and trace element variations

Harker diagrams of major element variations with SiO_2 in the LVF suite are shown in Fig. 10. Both MgO and CaO behave compatibly throughout the entire series, indicating the influence of *Ol* and/or *Cpx* removal. A group of three samples with ~10–11 wt % MgO (PLF2 and maar deposits) have accumulated significant *Ol*; the other lavas have MgO <7·5 wt %. The KVM series show the highest MgO values, and the early historical flows (e.g. the 1821 flow) and more evolved KVT rocks the lowest (~2·7 wt %). CaO also peaks in the most mafic KVM samples at 13·4 wt %.

Levels of Fe_2O_3* and TiO_2 show similar patterns to MgO and CaO until ~51 wt % SiO_2 when the data become more scattered, possibly reflecting the involvement of two distinct magma series (most clearly defined in the TiO_2 diagram). Elevated Fe_2O_3* (~15–16 wt %) and TiO_2 (up to ~2 wt %) contents are seen in the PLF1 and some KVT samples, and in several maar deposits; all these samples also show relatively high K_2O and P_2O_5 (Fig. 10). The latter are both incompatible in the LVF suite and there is no evidence for appreciable apatite fractionation, although there is a slight decrease in P_2O_5 with increasing SiO_2 in the high-K group.

The LVF lavas are highly aluminous (~14·5–20 wt % Al_2O_3). There is considerable scatter in Al_2O_3 contents, probably as a result of variations in *Plag* abundance, as the most *Plag*-rich sample is also the most aluminous (GKN3060; 20·2 wt % Al_2O_3). Despite this, Al_2O_3 appears to increase initially in the LVF lavas, until an inflexion at 50–51 wt % SiO_2 after which there is a general decline. This may also reflect multiple magma series, or possibly the onset of significant *Plag* fractionation.

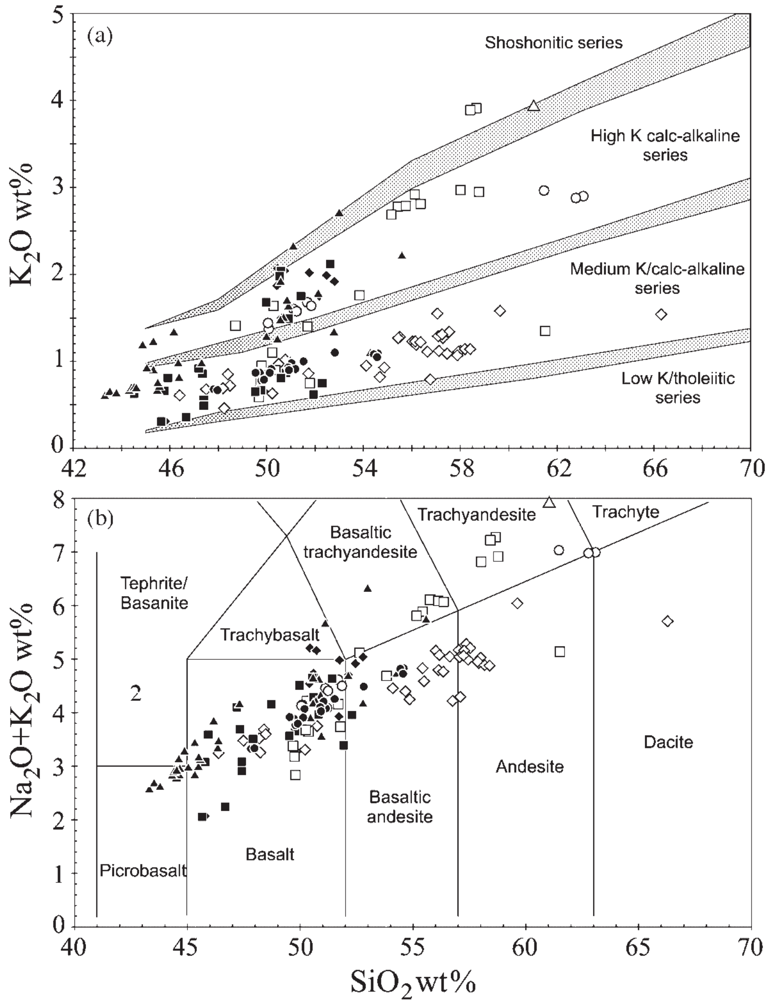

Fig. 8. (a) K_2O vs SiO_2 plot, after Peccerillo & Taylor (1976). Data are shown for the LVF [historical lavas (●), cinder cones (▲), PLFs (■) and maar deposits (◆)], Semeru (◇), Bromo–Tengger (□), Iliboleng (○) and Lewotolo (△). Data sources—LVF: this study; Semeru: Wahyudin (1991) and this study; Bromo: Van Gerven & Pichler (1995) and this study; Iliboleng and Lewotolo: S. A. Carn (unpublished data, 1996). Field boundaries are from Rickwood (1989). (b) Total alkali–silica (TAS) diagram, after Le Bas *et al.* (1986). Data and symbols as in (a). (See text for discussion.)

Variations in trace element concentrations with SiO_2 are shown in Fig. 11. Rb contents show similar patterns to K_2O, with the historical lavas, PLF2, PLF3 and most of the KVM samples forming a linear array with lower Rb (∼6–18 ppm), and a more diffuse group with higher Rb (∼21–77 ppm). The latter group comprises a small number of KVM and KVT samples at low SiO_2 and relatively high Rb that are closely related in space (samples with prefixes GCK, GKG, GMA and GKN, situated NE of Klakah; Fig. 2), and a cluster at higher SiO_2 (>50 wt %) consisting of the PLF1 series, the KVT lavas from the western LVF and many of the maar deposits (Fig. 11).

The relatively enriched, more evolved group of samples is also evident in the Ba, Zr, Nb, Y and (to a lesser extent) Sr plots (Fig. 11). Sr contents (∼300–600 ppm) show considerable scatter, as for Al_2O_3, suggesting the influence of *Plag* accumulation (e.g. Vukadinovic, 1993). The 'low-SiO_2, high-Rb' samples mentioned above also have slightly elevated Sr, suggesting that these magmas may have suffered similar contamination.

Ba contents show a wide range (∼200–1000 ppm) and also define a linear array with relatively low concentrations increasing with SiO_2, and a more enriched cluster at >50 wt % SiO_2. Concentrations in several PLF samples displaced below the linear array (Fig. 11) may have been diluted through the accumulation of ferromagnesian phenocrysts. Similar patterns are displayed by Zr, Y and Nb, with the divergent trend or enriched group at >50 wt % SiO_2 particularly evident. Zr contents are rather depleted in the low-SiO_2 samples (<50 ppm) but increase to ∼75 ppm at 54–55 wt % SiO_2 in the

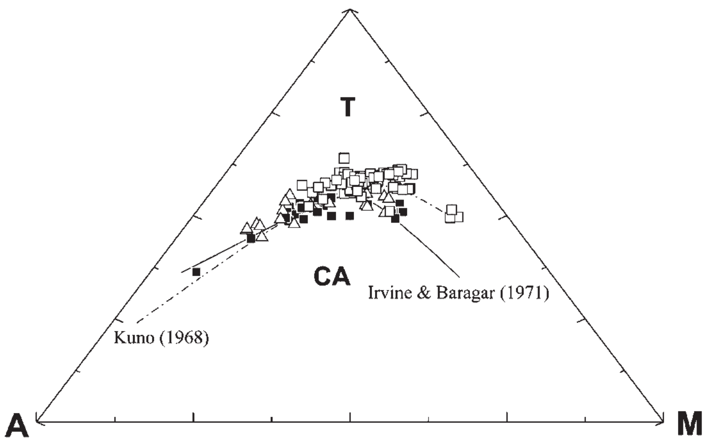

Fig. 9. AFM diagram [where A is $Na_2O + K_2O$, F is FeO_{tot} (total Fe as FeO) and M is MgO] showing lavas from the LVF (□), Semeru (■) and Bromo–Tengger (△). Data sources as in Fig. 8. Boundaries between the tholeiitic (T) and calc-alkaline (CA) fields from Kuno (1968) and Irvine & Baragar (1971) are shown.

most evolved historical lavas, and attain up to 226 ppm in some PLF1 and KVT rocks. Y varies from ~15 to 27 ppm with increasing SiO_2 in the linear array and up to ~58 ppm in the enriched group. Niobium contents are also relatively low in the LVF lavas, with many samples close to detection limits (Table 2) and the highest contents (10–11 ppm) recorded in a KVT sample and maar deposit. In the enriched group of samples, Zr, Y, Nb and possibly Rb and Sr all appear to decrease with increasing SiO_2 (Fig. 11).

Both Sc (~15–60 ppm) and V (~100–670 ppm) contents exhibit a steady decline with increasing SiO_2, although there is also evidence for an enriched group of samples at >50 wt % SiO_2, as observed in the incompatible element plots (Fig. 11). This compatibility of Sc and V in the LVF lavas attests to the influence of *Cpx* removal throughout the suite, with other deviations (particularly in Sc) probably attributable to varying modal proportions of the mineral.

Ni (<60 ppm) and Cr (<160 ppm) contents are both low in the LVF lavas, peaking in PLF2 samples that have visibly accumulated *Ol* (Fig. 11). Low Cr values imply minimal contamination by chromian spinel (e.g. in *Ol*) or by Cr-rich pyroxene. The group of KVT and PLF1 basalts that are relatively enriched in incompatible elements also have slightly elevated Ni (~30–40 ppm) but the values are still low. The historical lavas and some KVM samples are particularly depleted in Ni and Cr, even where Sc and V are elevated, which suggests that even the least evolved lavas have undergone some *Ol* fractionation. This is surprising given their low SiO_2 contents, and another possibility is that low Ni and Cr were inherited from the source.

Figure 12 shows N-MORB normalized trace element abundances in LVF lavas. All of the samples show a prominent trough at Nb, which is characteristic of subduction zone magmas. This depletion of Nb relative to the large-ion lithophile elements (LILE; e.g. Rb, Ba, K) is attributed primarily to two processes: (1) the addition of an LILE-enriched, Nb-poor fluid component to the mantle wedge; (2) the preferential retention of Nb in amphibole relative to other phases present in the mantle source (e.g. Borg *et al.*, 1997). Similar processes are inferred to explain the general depletion of the high field strength elements (HFSE) Zr, Ti and Y with respect to LILE in arc magmas (e.g. Pearce & Peate, 1995).

Inter-element trends for the LVF samples generally resemble a typical primary island-arc basalt (IAB) profile, but with more enriched values of most elements, although this is of course dependent on the IAB values used. Historical samples form the most homogeneous group, with notable enrichments in Rb, Ba, K, Pb, P, Ti and Y compared with IAB, and levels of Ba and Pb narrowly exceeding OIB (Fig. 12a). Ba enrichments in Javanese volcanic rocks are probably related to the input of Ba-rich oceanic sediments into the subduction zone (e.g. Plank & Langmuir, 1993).

The cinder cone lavas display varying levels of enrichment, although some of the variation will be due to crystal fractionation (Fig. 12b). KVT samples from the western LVF are typically most enriched, up to 10× primary IAB for Rb, and with relatively high values (compared with IAB) for all other elements except Sr (indicating *Plag* fractionation), exceeding or approaching ocean-island basalt (OIB) values in most cases. The KVM rocks and the cinder cones NE of Klakah (Fig. 2) generally represent the least enriched (i.e. most IAB-like) samples in the LVF. The latter have an interesting profile in Fig. 12b, showing significant Rb enrichment relative to IAB without a corresponding Ba anomaly. They are also

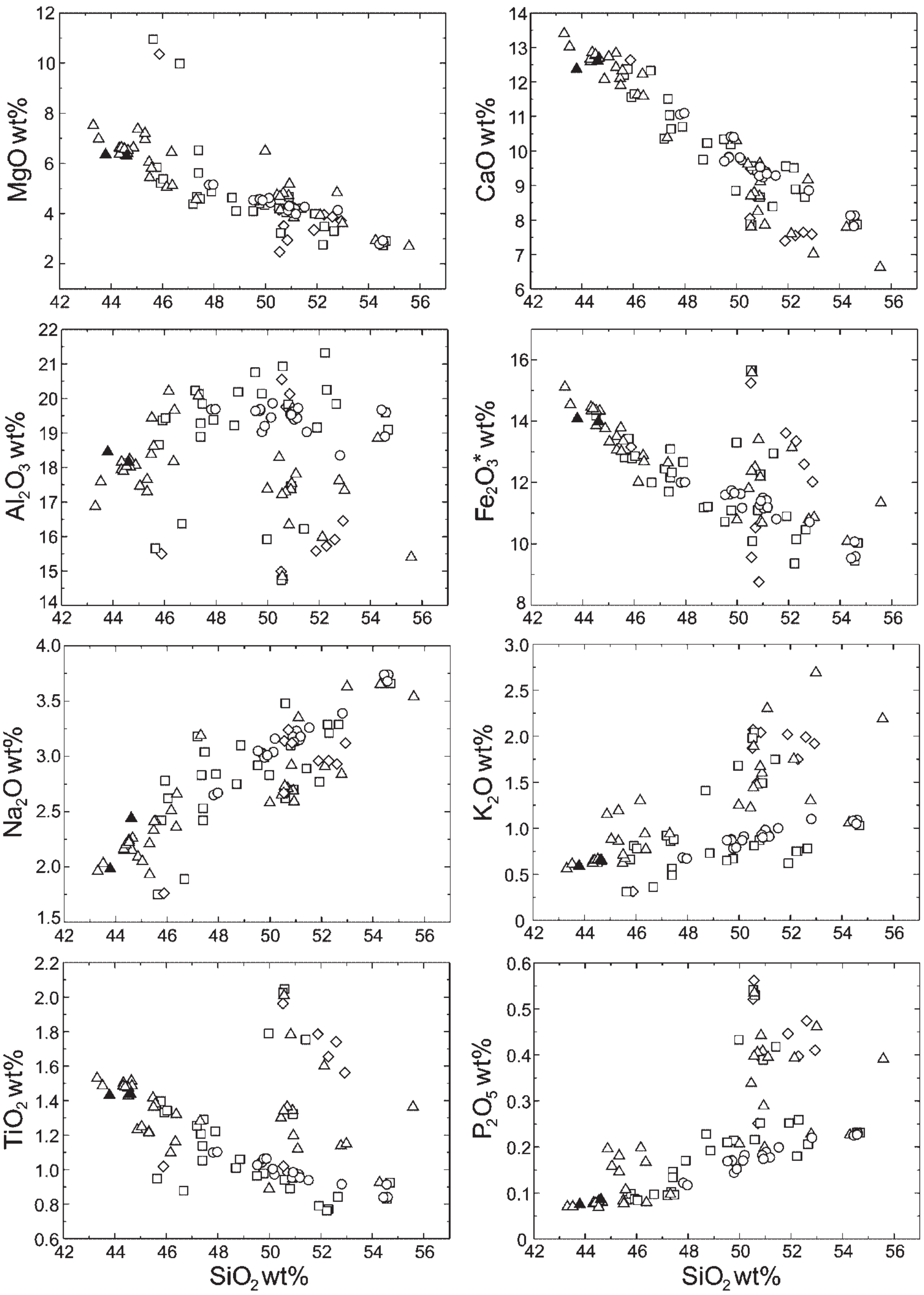

Fig. 10. Major element variation (vs SiO_2) in the LVF suite, showing historical lavas (○), cinder cones (△), PLFs (□) and maar deposits (◇); cinder or spatter cones within maars (▲) are now also distinguished. Fe_2O_3*, total Fe as Fe_2O_3.

depleted in Nb, P, Zr and, to a lesser extent, Sr, although enriched in Ti and Y, compared with IAB.

The PLF data display a similar range to the cinder cone samples, although there are two discrete groups rather than a continuum of compositions (Fig. 12c). The upper group is highly enriched in Rb, Ba, K, Pb, P, Zr, Ti and Y with respect to typical IAB and consists of the PLF1 series; these samples also show a small negative Sr anomaly similar to the KVT cones in the western LVF. The less enriched group comprises the PLF2 and PLF3 series, with the former exhibiting slight depletions in Nb, P and Zr, and enrichments in Ti and Y, relative to IAB

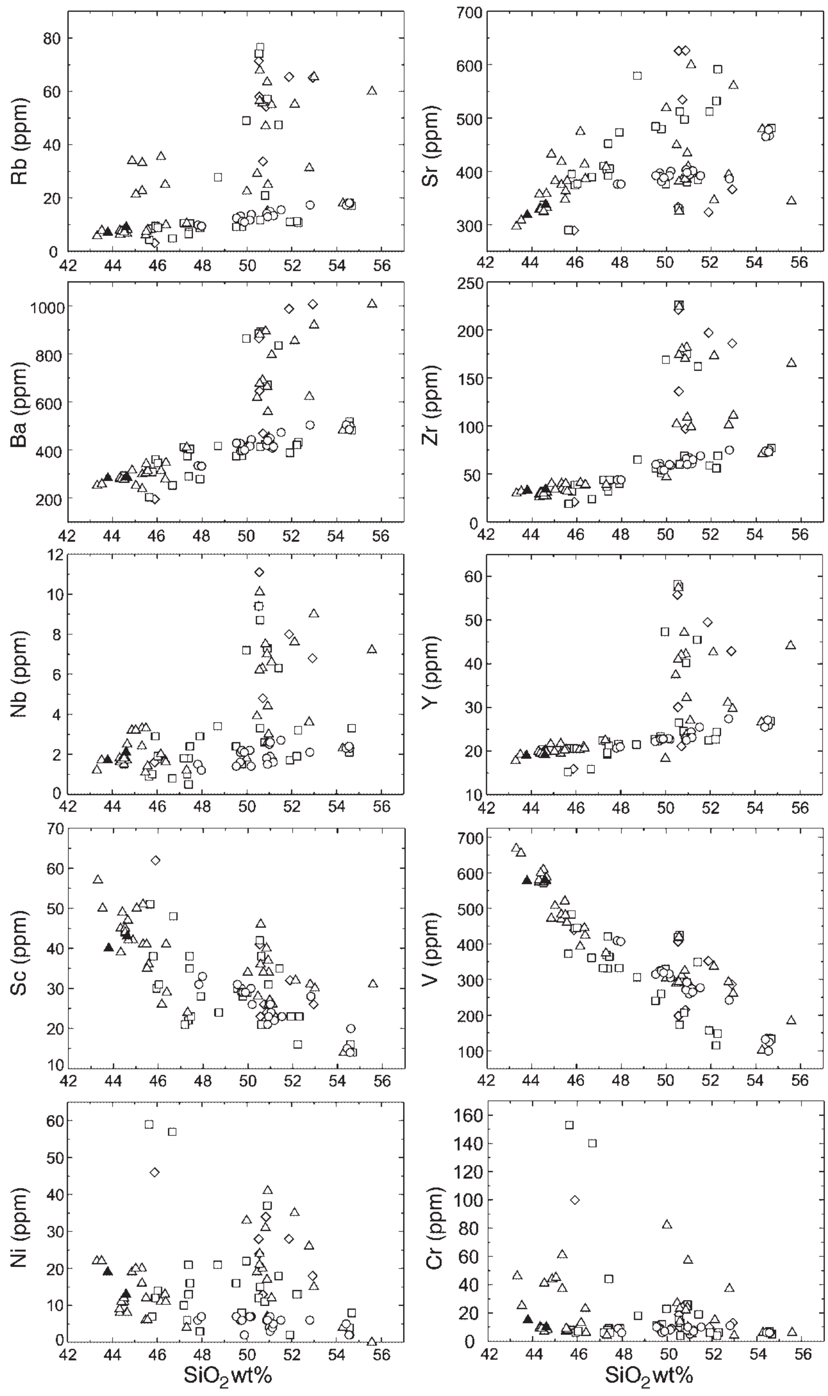

Fig. 11. Trace element variation (vs SiO_2) in LVF lavas. Symbols as in Fig. 10.

(Fig. 12c). The only element that appears to be relatively constant throughout the suite is Sr, which is typically at or close to typical IAB abundance.

In summary, all of the LVF samples are enriched in Rb, Ba, K, Pb, Ti and Y to some degree relative to a typical primary IAB. Most of the lavas carry the typical subduction signature of Nb and HFSE depletion and LILE enrichment, with the cinder cone and PLF samples showing the greatest variability. Several of the KVM and PLF2 samples show low abundances of Nb, P and Zr relative to typical primary IAB and N-MORB, but without corresponding depletions in Ti and Y, and some cones

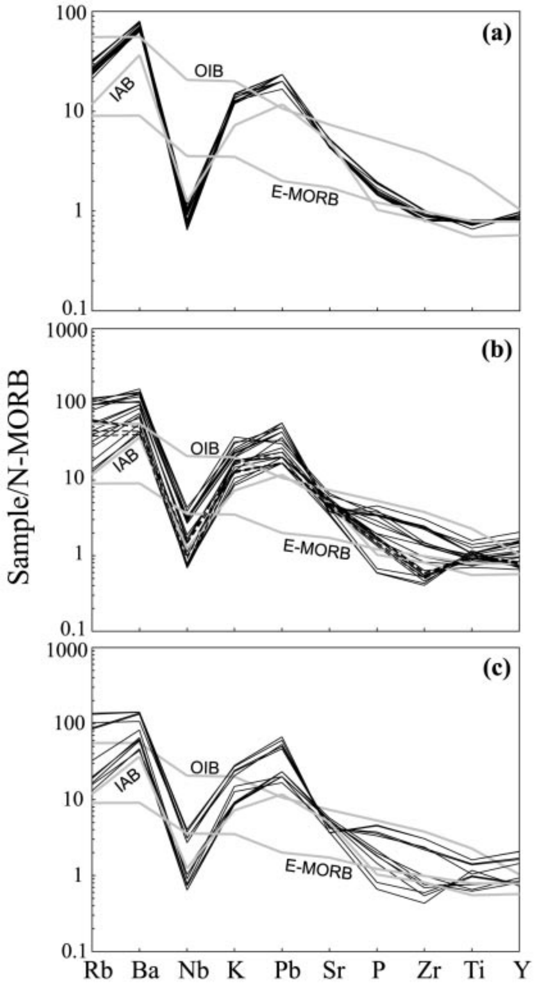

Fig. 12. N-MORB-normalized trace element diagrams for (a) historical lavas, (b) cinder cones (the cinder cone cluster NE of Klakah is distinguished by dashed lines), and (c) PLFs. Samples with Nb or Pb below or close to detection limits (Table 2) are excluded. Typical ocean-island basalt (OIB), primary island-arc basalt (IAB) and E-MORB trends are shown for reference. Normalizing values, OIB and E-MORB compositions from Sun & McDonough (1989); IAB is sample ID16 from Nye & Reid (1986), a primary arc basalt from the Aleutian Islands.

appear to preserve localized geochemical heterogeneities such as enrichment in Rb relative to Ba. Abundances of Rb, P and Zr show the greatest, and Sr the smallest, range. A similar consistency of Sr abundance is seen in lavas from Gunung Slamet in central Java (e.g. Vukadinovic & Sutawidjaja, 1995).

Sr isotopes

The limited number of Sr isotope ratios available occupy a fairly narrow range (0·7042–0·70445; Table 2), with the lowest values close to the Sunda arc minimum (e.g. Whitford, 1975). This is consistent with the general decline in $^{87}Sr/^{86}Sr$ from West Java to Bali (Fig. 1).

The $^{87}Sr/^{86}Sr$ ratios do not correlate with SiO_2 or Rb/Sr, although the highest ratio occurs in a KVM sample with anomalously high Rb and relatively high Rb/Sr (GCK2961; Table 2), which suggests source enrichment in this region. The lowest ratios occur in the historical lavas.

Principal component analysis

To clarify the complex patterns presented on binary diagrams by the large number of samples and elements analysed, the major and trace element XRF data from the LVF suite have been subjected to principal component analysis (PCA). PCA locates the directions of maximum variance in a multivariate dataset by finding the eigenvalues and eigenvectors of the data correlation matrix, and selects the combination of the initial variables responsible for this variance (e.g. Le Maitre, 1968; Albarède, 1995). In this analysis the historical lavas, cinder cones and PLFs have been treated as separate groups.

The first three principal components (PCs) of the historical lava data, which represent 85% of the total variance, are depicted in Fig. 13. The horizontal spread of these data (PC1) is generally related to the eruption age of the lavas, with PC2 probably picking out subtle variations in phenocryst content.

At opposite extremes of the PC1 axis, we find the oldest (1821) and youngest (1898) historical samples. The former correlate with the incompatible elements (Rb, Zr, Ba, etc.) and relatively evolved components (SiO_2, K_2O, Na_2O; e.g. alkali feldspar), whereas the latter correlate with a 'pyroxene and Fe–Ti oxide' component (i.e. MgO, Fe_2O_3, TiO_2, CaO, V, Sc; Fig. 13). This probably implies that the magma chamber feeding the 19th-century eruptions at Lamongan was stratified, with the relatively evolved basalts at the top of the chamber erupted first (1821) and the more mafic magmas at the chamber base, enriched in dense ferromagnesian phenocrysts, erupted last (1898) and at the lowest altitude (Fig. 3).

Lavas erupted in 1864 cluster at the centre of the plot (Fig. 13), i.e. closest to the 'average' composition of historical Lamongan basalts. Significantly, Al_2O_3, Ni, Cr and Nb appear to exert little influence on the chemistry of erupted lavas, except possibly through minor variations in *Plag* content, suggesting that the abundance of these variables (i.e. high Al_2O_3, low Ni, Cr, Nb) was controlled primarily by the 'source' or in this case the magma supplied to the chamber.

A corollary of using PCA is that lavas of similar overall composition, and by inference of similar age, will cluster together in PC space. This is of use at Lamongan, where there is poor age control on several samples. The plot

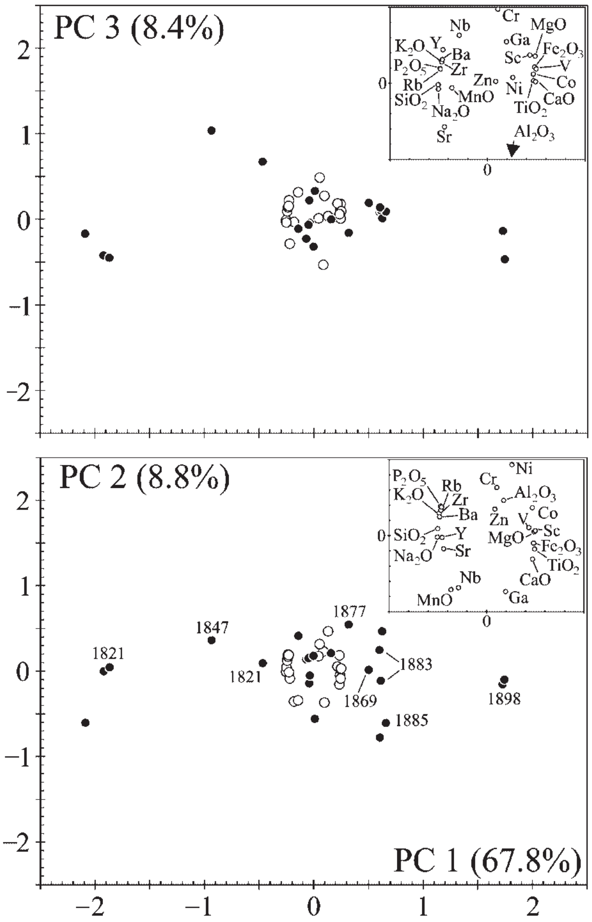

Fig. 13. Principal component analysis (PCA) of major and trace elements in 19th-century lavas from Lamongan volcano, showing the first three principal components (PCs). ○, positions of the initial variable axes in PC space (see inset for key); ●, historical lava samples (several samples are labelled with eruption ages). Units on both axes are standard deviations. The first two components account for ~77% of the total variance.

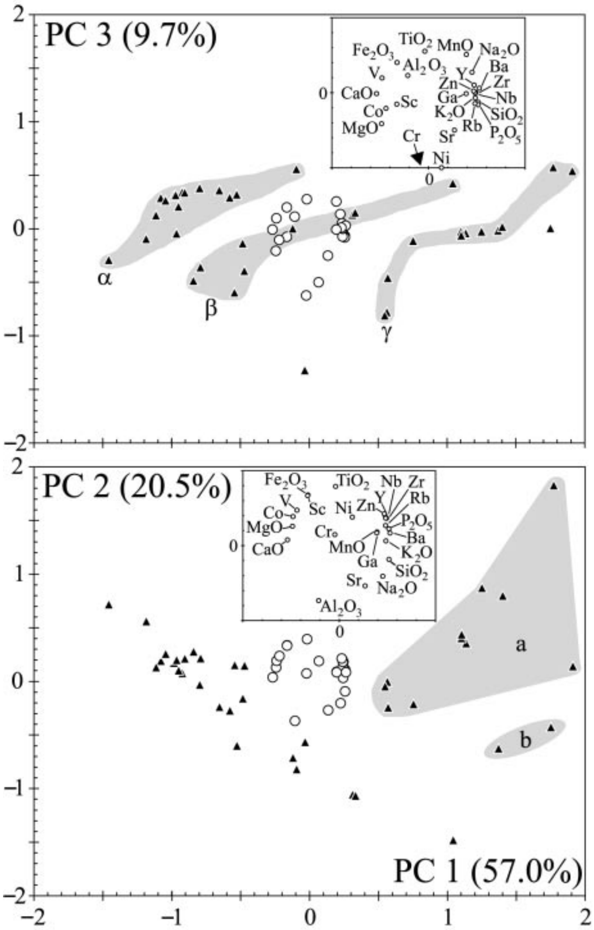

Fig. 14. PCA of major and trace elements in LVF cinder cone samples, showing the first three PCs, plotted as in Fig. 13. ▲, cinder cone samples. The first two components account for 77·5% of the total variance. In the lower plot, group a comprises the KVT samples from the western LVF; group b comprises two K-rich (shoshonitic) samples. In the upper plot, the following groups are demarcated: α, most of the cones to the north and south of LTT; β, the cones in the 'transition zone' west of LTT; γ, the KVT cones in the western LVF. (See text for discussion.)

of PC3 against PC1 (Fig. 13) splits the samples into a 'Y'-shaped array, with the 1821 samples grouping with sample LAM1207 on the lower 'arm'. This latter sample was thus probably erupted at a similar time to the former, but from a different vent (Fig. 3). Similarly, samples LAM1261 (1847 flow) and LAM1563 (1821 flow?) also have similar characteristics (e.g. relatively high Nb contents) and hence may in fact be part of the same flow field (probably 1847; Fig. 3).

The cinder cone samples form a broadly L-shaped array in the plot of the first two PCs (Fig. 14), and the first three PCs account for ~87% of the variance. This L-shaped pattern is often observed for suites of lavas from individual volcanoes, with picritic and differentiated flows occupying separate 'arms' and common compositions clustering at the apex (e.g. Albarède *et al.*, 1997). In Fig. 14, one limb is composed of the KVT cones from the western LVF (west of the roughly north–south lineament defined by the three lake-filled maars immediately east of Klakah; Fig. 2) and two transitional high-K–shoshonitic samples (GTE288 and GAP1070). The KVM series and KVT samples from the central and eastern LVF form the other limb, with the younger cones plotting towards the left-hand side (Fig. 14). There is no appreciable clustering of samples at the 'apex', indicating that the LVF cones constitute two distinct magma series with little compositional overlap between them. However, several of the lavas that do plot in the region of the apex (GRG14071/2, GCK2960, GKN3060) are derived from cones situated close to the boundary between the compositionally distinct cones of the western LVF and the rest of the complex (Fig. 2).

The western LVF samples are predominantly controlled by K_2O, P_2O_5 and the incompatible elements, whereas the spread of compositions in the other lavas correlates with a CaO–MgO–Fe_2O_3–Sc–V–Co component (*Cpx* or possibly amphibole) and a SiO_2–Na_2O–Al_2O_3–Sr component (*Plag*), the former predominating in the KVM samples (Fig. 14). As observed in the historical lavas, Ni and Cr are not strongly correlated with the ferromagnesian component and plot at the centre of the diagram, suggesting minimal influence of mantle phases (Ni-rich *Ol*, Cr-rich pyroxene) on the major compositional trends and reflecting the overall low Ni and Cr contents of the suite. These elements exert more influence in the PC3 plot (Fig. 14), which probably reflects minor variations as a result of *Ol* accumulation in some magmas. Also in the PC3 diagram, the Al_2O_3 axis plots towards the pyroxene component, indicating the significance of Al-rich pyroxene in these lavas.

The spatial variation of magma composition in the LVF is also subtly manifested in the PC3 plot (Fig. 14), wherein three distinct geographical groups of cinder cones can be recognized. One group collects most of the cones on the northern and southern flanks of the LTT edifice (α; Fig. 14), which show a strong correlation with Fe_2O_3 and TiO_2. Another assemblage (β) contains the samples from a narrow region to the west of LTT and east of the three lake-filled maars (GMA5070, GCK2961/2960/1071, GKG136, GKL256, GRG14071/2, GKN3060; Fig. 2). This acts as a 'transition zone' between the previous group and the third group (γ), which contains the KVT samples from the western LVF. This last group seems to correlate with Sr and the incompatible elements, and possibly Ni and Cr.

The PLF samples also define an L-shaped array in PC space (Fig. 15), with the PLF1 group clearly distinguished. These lavas correlate with the axes for K_2O, P_2O_5 and the incompatible elements in the PC1–PC2 plot, whereas the PLF2/3 trend is controlled by a ferromagnesian component (*Ol*, *Cpx*) and *Plag* (SiO_2, Al_2O_3, Na_2O, Sr). Thus the PLF1 samples, which come from localities in the western LVF (Fig. 2), have similar overall characteristics to the KVT cones in the same region of the field.

Contrary to the historical lavas and cinder cones, the PLFs show a more robust correlation between Ni, Cr and MgO. This indicates that the Ni and Cr budget is primarily controlled by the accumulation of phenocrysts rich in compatible elements (e.g. *Ol*) in the PLFs, and by the source in the historical lavas and cinder cones.

To summarize, many latent geochemical features of the LVF lavas are revealed by PCA. Spatial heterogeneities in magma composition are particularly apparent, with a clear distinction evident between lavas from the eastern and western parts of the LVF, and transitional samples with intermediate compositions. Contents of Rb, Ba, Y, Zr, K, P, ±Nb are interrelated in all samples, implying that these elements behaved incompatibly during magma evolution. Compatibility of Sr in *Plag* is indicated by the general correlation of Sr with the *Plag* component on plots of the first two PCs. Similarly, the general lack of correspondence between Ni, Cr and the ferromagnesian phases (except in the PLFs) attests to the low concentrations of these elements in the LVF suite (Fig. 11), which are probably a feature of the source magmas.

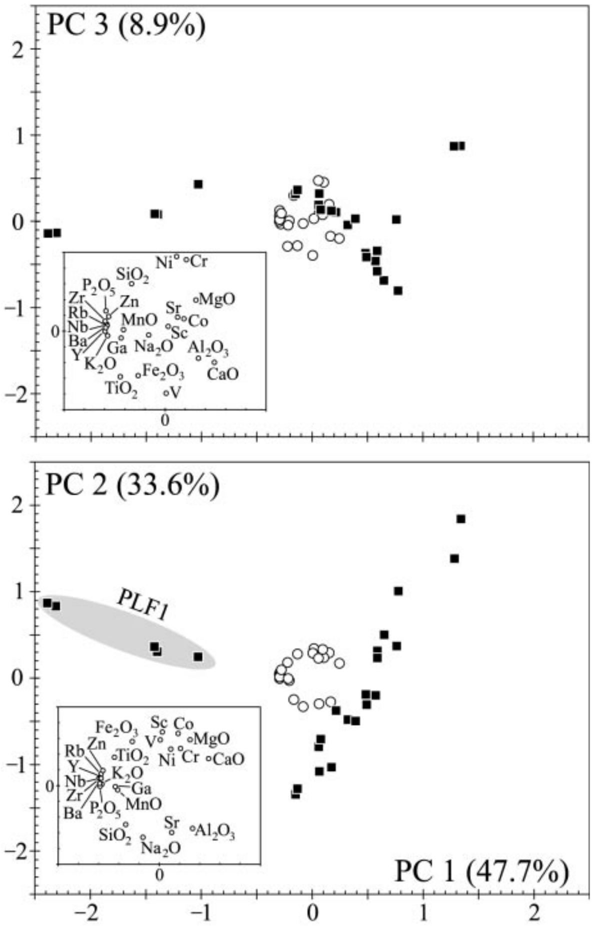

Fig. 15. PCA of major and trace elements in LVF prehistoric lava flows, showing the first three PCs, plotted as in Fig. 13. ■, the PLF samples. The first two components account for 81·3% of the total variance. PLF1 and PLF2/3 samples are clearly separated in these diagrams. (See text for discussion.)

FRACTIONAL CRYSTALLIZATION IN THE LVF LAVAS

Major elements

The results of PCA suggest that fractional crystallization of *Ol*, *Cpx*, *Plag* and Fe–Ti oxides may be responsible for much of the compositional variation within individual lava suites in the LVF. Mass balance calculations (e.g. Bryan *et al.*, 1969) have been employed to investigate this further, using mineral analyses from this work (Tables 4–6) with the exception of apatite (from Wood *et al.*, 1995). Following Defant & Nielsen (1990), we have used 0·1 as an upper bound for the sum of the squares of the residuals (Σr^2), as values greater than this point to the involvement of other processes, such as assimilation or magma mixing, in addition to crystal fractionation during magma evolution.

Selected results of mass balance calculations are given in Table 8. Predicted mineral assemblages are generally consistent with the observed modal mineralogy (Table 3), despite the evidence for crystal disequilibrium and accumulation (e.g. Fig. 6). It is thus unlikely that magma evolution in the LVF involved pure fractional crystallization, implying the removal of fractionating phases from the evolving melt, but that it entailed some mixing of phenocrysts and less evolved liquids. This is also implied by the generally scattered data in the Harker variation diagrams (Fig. 11).

Mass balance modelling reveals potential genetic links between the KVM cones on the northern and southern flanks of LTT (east of sample ALA1161; Fig. 2), the entire series of historical lavas from Lamongan, and recent products of Semeru (e.g. sample SEM1607 from the February 1994 pyroclastic flow deposits; Table 2). These samples form a continuous sequence related by crystallization of variable proportions of *Cpx* + *Plag* + *Mag* + *Ol* (Table 8, numbers 1–7 and 16). On the basis of these calculations, samples GRJ288 or ALA1161 would be likely candidates for 'parental' magmas for recent lavas from Lamongan and Semeru.

Orthopyroxene (*Opx*) may enter the assemblage in the more evolved samples (e.g. LAM1561, SEM1607), being a common constituent of recent lavas at Semeru (e.g. the 1941–1942 lava flow; Table 2). There is little evidence for significant removal of *Opx* from the LVF suite, and its occurrence is restricted to the unstable cores and rims of *Cpx* crystals in the more evolved samples.

No acceptable Σr^2 values were obtainable between the recent lavas and the KVT cones in the western LVF, indicating either that the two magma series are not genetically linked or that other processes were involved in the genesis of the KVT cones. Good matches were often achieved for all elements except the alkalis (Na_2O and K_2O), suggesting that mixing with an alkali-enriched (metasomatic?) component may link the two series, although this has not been tested. However, the least evolved sample from the western LVF (GOO13072; Fig. 2) is an acceptable parental composition for most of the KVT cones in that area and also for recently erupted lavas from Bromo (sample BRO1, erupted in March 1995; Table 2) to the west of the LVF (e.g. Table 8, numbers 8–10). A possible problem with this model is that the fractionating assemblage involves considerable amounts of *Cpx* (Table 8), which is only sparsely present in the lavas.

Several other clusters of cinder cones appear related to a common parental magma. Lavas from the array of collinear vents to the NW of LTT (GTU298–GGI2661; Figs 2 and 3) can all be derived from sample GPG2660, collected from a prehistoric lava flow (e.g. Table 8, numbers 11–13). Morphological evidence suggests that these vents and flows are of different ages and were probably emplaced along a roughly NW–SE-aligned fissure that has also produced maar-forming eruptions (Fig. 2; Carn, 2000). However, their related chemistries could indicate a contemporaneous, fissure-style eruption event, although the progressive exploitation over time of an eruptive fissure supplied by an evolving magma chamber would also be a feasible scenario.

The group of cones (KVM and KVT) to the west of the historical lava flow field on the flanks of Lamongan and east of the three lake-filled maars (Fig. 2) is also compositionally interrelated (e.g. Table 8, numbers 17 and 18). These samples, which were 'transitional' in the PCA diagram (Fig. 14), cannot, however, be related to any of the other cone clusters by a simple fractional crystallization process. As for the KVT cones in the western LVF, alkali contents are the main stumbling block in the mass balance calculations, and magma mixing may have been involved.

Calculations on the PLF samples suggest genetic links within and between the PLF2 and PLF3 series, involving relatively high proportions of *Ol* in the fractionating assemblage (e.g. Table 8, numbers 14 and 15). Fractionation between the PLF1 and PLF2/3 samples could not be successfully modelled, in accord with the orthogonal relationship between these two groups in PC space (Fig. 15).

Trace elements

Fractionation of trace elements was modelled using the Rayleigh fractionation equation, $C_L = C_O F^{(D-1)}$; where C_L and C_O are the concentrations of a given element in the daughter and parental liquids, respectively, F is the proportion of residual liquid and D is the bulk crystal–liquid distribution coefficient for that element (Shaw, 1970). Appropriate elemental partition coefficients (K_d values) were obtained from the literature (Table 9), with the crystallizing phases and proportions determined from the mass balance calculations (Table 8).

This simple model generally reproduced the trace element contents of the modelled daughter liquids to an acceptable degree (Table 9). The only element that was consistently overestimated was V; this suggests that the K_d used for V in *Cpx* (0·8) may have been too low.

Table 8: Results of major element least squares mass balance calculations (e.g. Bryan et al.*, 1969) on LVF samples*

	KVM cones—historical lavas—Semeru lavas						
	1	2	3	4	5	6	7
Parent:	GRJ288	ALA1161	BUK1407	LAM18981	LAM18831	LAM1261	LAM1561
Daughter:	ALA1161	BUK1407	LAM18981	LAM18831	LAM1261	LAM1561	SEM1607
SiO_2 range (%):	43·5–44·3	44·3–45·4	45·4–47·6	47·6–49·4	49·4–52·4	52·4–54·1	54·1–56·5
%							
OL	1·7	1·5	0·5	2·2	3·0	1·9	3·0
CPX	6·0	4·8	10·3	6·8	1·8	6·0	1·1
PLAG	5·6	5·4	8·4	18·4	20·5	3·4	13·7
MAG	2·2	2·6	4·2	3·2	3·7	1·7	2·6
F	84·5	85·7	76·6	69·5	71·0	87·0	79·6
Σr^2	0·02	0·007	0·08	0·003	0·006	0·02	0·02
	KVT cones in west LVF; vents to NW of LTT						
	8	9	10	11	12	13	
Parent:	GOO13072	GOO13072	GOO13072	GPG2660	GPG2660	GPG2660	
Daughter:	GJK3070	GBR3070	BRO1	GGI2661	GPN2861	GTU298	
SiO_2 range (%):	50·6–52·3	50·6–52·6	50·6–56·5	44·1–45·3	44·1–47·0	44·1–45·5	
%							
OL	2·8	2·0	1·4	1·2	2·6	1·4	
CPX	5·1	7·2	15·3	7·5	18·4	10·8	
PLAG	19·1	16·7	23·0	6·9	14·1	4·5	
MAG	1·6	2·3	5·6	3·1	6·5	3·7	
AP	0·3	0·2	0·2	—	—	—	
F	71·1	71·6	54·5	81·3	58·4	79·6	
Σr^2	0·03	0·09	0·06	0·05	0·01	0·03	
	PLF2-PLF3; KVM north and south of LTT; cones to west of LTT						
	14	15	16	17	18		
Parent:	RWG116	RWG116	GRJ288	GMA5070	GCK2961		
Daughter:	KPG1107	LAO1207	GKK1107	GKG136	GKG136		
SiO_2 range (%)	47·3–49·4	47·3–51·8	43·5–44·1	44·8–45·3	44·9–45·3		
%							
OL	9·2	11·4	1·2	1·5	1·3		
CPX	9·0	9·5	5·0	1·8	6·8		
PLAG	25·5	36·2	5·4	5·3	6·2		
MAG	2·3	3·4	1·8	1·4	1·0		
F	54·1	39·3	86·4	89·7	85·0		
Σr^2	0·01	0·1	0·01	0·02	0·08		

OL, olivine; CPX, clinopyroxene; PLAG, plagioclase; MAG, magnetite; AP, apatite; F, liquid fraction (all in wt %). Σr^2, sum of squares of residuals. Sample analyses were recalculated to 100% before modelling.

Table 9: Rayleigh fractionation modelling of trace elements in LVF rocks (all concentrations in ppm)

	Parent GRJ288	Bulk *D*	Daughter ALA1161	Model	Parent ALA1161	Bulk *D*	Daughter BUK1407	Model
Rb	7·8	0·16	6·7	9·0	6·7	0·17	8·0	7·6
Sr	308	0·64	358	328	358	0·68	382	376
Y	19·2	0·19	20·2	22·1	20·2	0·16	20·4	23·0
Zr	32	0·10	27	37·3	27	0·11	32	31·0
Nb	1·7	0·03	1·7	2·0	1·7	0·03	1·4	2·0
Ba	258	0·67	283	273	283	0·70	313	297
Sc	50	1·27	47	47·7	47	1·20	36	45·6
V	655	0·30	578	739	578	0·26	460	649
Cr	25	8·02	9	7·5	9	7·23	8	3·4
Co	52	1·31	43	49·3	43	1·42	39	40·2
Ni	22	2·02	8	18·5	8	2·08	6	6·8
Zn	77	0·24	72	87·6	72	0·22	79	81·4
Ga	18	0·14	17	20·8	17	0·12	16	19·5
	Parent LAM18981	Bulk *D*	Daughter LAM18831	Model	Parent GOO13072	Bulk *D*	Daughter GJK3070	Model
Rb	9·9	0·12	12·9	13·6	56·4	0·10	55·1	76·8
Sr	376	0·93	397	385	381	0·99	346	383
Y	20·7	0·11	22·7	28·6	41	0·09	42·6	55·9
Zr	44	0·07	61	61·7	174	0·04	173	241
Nb	1·5	0·04	1·6	2·1	6·2	0·04	7·6	8·6
Ba	335	0·96	427	339	676	0·29	854	861
Sc	31	0·78	30	33·6	36	0·60	32	41·2
V	409	0·17	324	553	293	0·14	337	394
Cr	9	4·71	9	2·3	23	3·78	15	8·9
Co	37	0·91	33	38·3	37	0·75	35	40·3
Ni	6	1·37	6	5·2	21	1·41	35	18·3
Zn	87	0·15	90	119	116	0·15	123	155
Ga	19	0·08	19	26·5	20	0·07	19	27·5
	Parent GPG2660	Bulk *D*	Daughter GTU298	Model	Parent GPG2660	Bulk *D*	Daughter GGI2661	Model
Rb	7·6	0·19	7·4	9·2	7·6	0·20	6·1	9·0
Sr	329	0·48	363	371	329	0·67	347	353
Y	19·5	0·25	20·2	23·2	19·5	0·19	20·1	23·1
Zr	30	0·15	40	36·4	30	0·12	33	36·1
Nb	1·7	0·03	3·3	2·1	1·7	0·03	1·1	2·1
Ba	278	0·18	342	336	278	0·57	304	304
Sc	49	1·88	35	40·0	49	1·33	41	45·7
V	599	0·77	481	632	599	0·30	520	693
Cr	9	5·07	9	3·5	9	8·25	7	2·0
Co	42	1·48	39	37·6	42	1·29	42	39·5
Ni	11	1·93	12	8·9	11	1·67	6	9·6
Zn	76	0·26	77	90·0	76	0·21	78	89·7
Ga	16	0·18	17	19·3	16	0·14	17	19·2

Bulk *D* is bulk distribution coefficient for corresponding modelled crystallizing assemblage in Table 8. Trace element distribution coefficients from Villemant *et al.* (1981), Dunn & Sen (1994) and Jeffries *et al.* (1995).

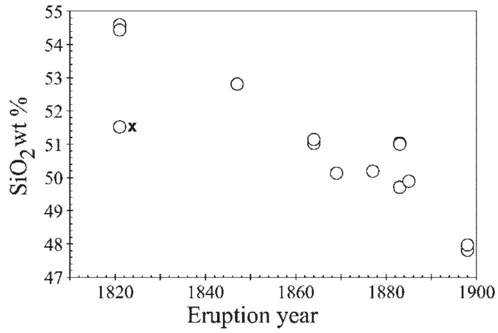

Fig. 16. Variation of SiO_2 content with time in historical lava flows from Lamongan volcano. The sample marked 'X' (LAM1563) may actually have been erupted in 1847, as suggested by the PCA results.

Measured K_d values for V in amphibole are high (∼6 for basalts; e.g. Vukadinovic & Sutawidjaja, 1995), but there is minimal petrographic evidence for amphibole fractionation in these lavas.

Fractional crystallization is thus a potentially viable process to explain the major and trace element variations in separate series of LVF lavas. *Plag* and/or *Cpx* dominate most of the calculated assemblages, with *Ol* fractionation apparently significant in the evolution of the PLFs (Table 8). The crystallization sequence in the evolving magmas is difficult to pinpoint using petrographic evidence. On the basis of observed inclusion relationships, phenocryst sizes and degree of disequilibrium, a likely succession in the historical lavas and KVM samples would be *Ol* followed by *Cpx* and/or *Mag*, followed by *Plag*, late *Opx* and a late phase of *Mag* growth (or pyroxene breakdown) to produce the observed rims on *Cpx* phenocrysts. Both the KVT and PLF2 rocks show evidence for crystallization of *Plag* before *Cpx*.

With the exception of the KVT and PLF1 samples, the LVF lavas are generally highly phyric, with widespread evidence for phenocryst disequilibrium (e.g. Fig. 6). These observations raise the question that the compositions of some LVF lavas could be the product of essentially random mixing of phenocrysts and liquid, and hence bear little relation to a true liquid line of descent. However, the regular decrease in SiO_2 (and increase in MgO) observed in the sequence of 19th-century lava flows erupted from Lamongan (Fig. 16) argues against such random sampling, at least in the historical lavas.

SPATIAL GEOCHEMICAL VARIATIONS

Compositions of lavas erupted from cinder cones in the LVF appear to vary systematically with vent location, as documented in the preceding sections. Possible origins of this variation have been explored using incompatible element ratios, which are unaffected by fractional crystallization.

In Fig. 17, Zr/Y and Zr/K ratios are used to discriminate between the various geochemically distinct cinder cone clusters. Zr and Y are both relatively immobile in aqueous fluids (e.g. Tatsumi *et al.*, 1986) and hence can provide information on the mantle source region of the lavas without contamination by fluids from the subducting slab. In the Zr/Y plot, the data bunch in a similar fashion to that observed in the PCA diagram (Fig. 14), although with slightly more overlap between groups. There is a clear separation between the KVT cones in the western LVF at high (>2·5) Zr/Y, and the eastern LVF cones at low (<2) values, with a 'transitional' group falling at intermediate ratios. The two shoshonitic samples also have high Zr/Y.

A possible explanation for the observed variation in Zr/Y ratios across the LVF is that the parental magmas for each cone group formed at different depths in the mantle wedge. Small degrees of melting at high pressures (>15 kbar) could result in elevated Zr/Y owing to retention of Y in garnet and *Cpx* (e.g. Tatsumi & Eggins, 1995), which would suggest a deeper source for the cones in the western LVF and the shoshonitic lavas (Fig. 17a). This would be consistent with the elevated K_2O contents of these samples, as it is well known that K_2O in erupted lavas often correlates positively with depth to the subducting slab in arc settings (e.g. Dickinson, 1975). What is not clear, however, is why magmas apparently generated at different depths should have erupted at similar distances from the arc front in the LVF.

Ratios of immobile to mobile incompatible trace elements (e.g. Zr/K) are more difficult to interpret, because of the effects of metasomatism of the mantle source on the mobile components. Zr/K ratios in the LVF cinder cones, however, show similar patterns to Zr/Y ratios, albeit with a few notable differences (Fig. 17b). As in the Zr/Y plot, the data cluster in spatial groups with the KVT cones in the western LVF displaying the highest ratios, but six of the 'transitional' samples and the shoshonitic rocks are displaced to lower Zr/K than the cones from the eastern LVF. This could be interpreted as the effect of addition of a K-rich or metasomatic component (e.g. slab-derived fluids; Vukadinovic & Nicholls, 1989) to the samples with low Zr/K, or that these lavas were produced by the melting of a metasomatic layer in the mantle beneath Java. If so, then Zr/K variations in the other LVF lavas may be due to varying degrees of metasomatism of their respective source regions, with the KVT cones in the western LVF associated with the least metasomatized mantle source.

HOW PRIMITIVE ARE THE PARENTAL MAGMAS IN THE LVF?

According to the results presented above, there are at least two distinct LVF lava series: an older high-K suite

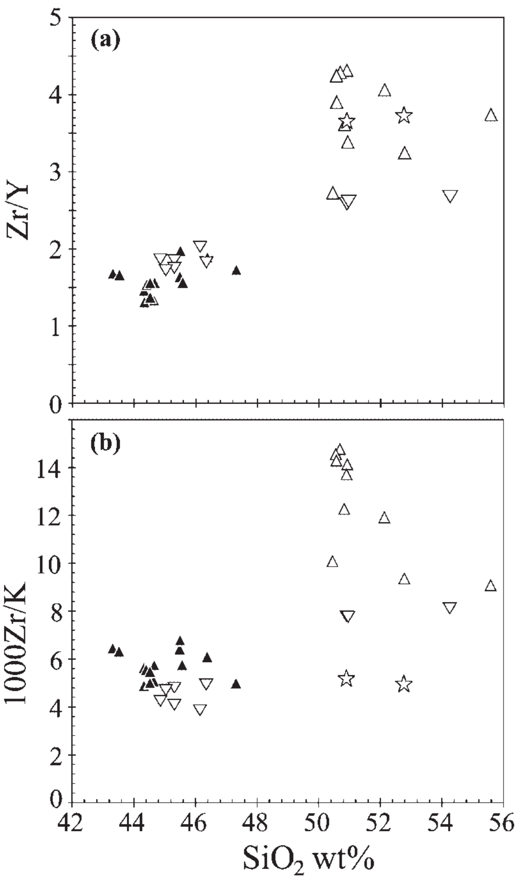

Fig. 17. Variation of trace element ratios in LVF cinder cones. (a) Zr/Y vs SiO_2. The data are divided geographically into: cones in the eastern LVF [▲; represents all samples approximately east of and including ALA1161 in Fig. 2, plus sample GGI2661 but omitting the shoshonitic lavas (see below); i.e. group α in Fig. 14]; cones east of Klakah (Fig. 2) but west of the previous group (▽; includes samples with prefixes GRG, GCK, GKG, GKL, GMA, GKN; i.e. group β in Fig. 14); KVT cones in the western LVF (△; represents all samples west of and including GMI15072; i.e. group γ in Fig. 14); and the transitional high-K–shoshonitic samples GTE288 and GAP1070 (open star). (b) 1000 × Zr/K vs SiO_2. Data and symbols as in (a). Scatter in these plots is probably partly due to variations in phenocryst content. (See text for discussion.)

(the KVT cones in the western LVF and the PLF1 series) and a calc-alkaline or medium-K suite (the KVM cones and historical lavas). A third series (GMA5070, GKG136, GCK2961, etc.; Fig. 2) possibly resulted from the mixing of these two end-member compositions and was erupted from vents situated spatially between them. The LVF high-K and medium-K series display genetic lineage with the recent lavas of Bromo and Semeru–Lamongan, respectively, and hence have the potential to contribute significantly to our understanding of magma genesis in the region.

Mass balance calculations (Table 8 and 9) suggest that samples GRJ288 and ALA1161 are close to parental compositions (i.e. the most primitive lavas recognized in the suite; Woodhead, 1988) for the medium-K series but, as discussed below, they are unlikely to represent true primitive or primary magmas. These samples are derived from two of the morphologically youngest prehistoric vents in the LVF (Carn, 2000), on the northern flanks of LTT (Fig. 2). Several features of these lavas indicate that they closely approximate true liquid compositions. Relative to many other LVF lavas, they are phenocryst poor (e.g. Table 3) and show few disequilibrium textures in the phenocrysts present (e.g. Table 7). In the case of sample ALA1161, the narrow range of *Ol* compositions plots within the high-pressure equilibrium field if it is assumed that $Fe_2O_3/FeO = 0{\cdot}2$ in the host liquid (Fig. 6), indicating a probable absence of xenocrystic or accumulative *Ol*. However, the modelled parental magma for the high-K suite (GOO13071) probably has accumulated *Ol* (Fig. 6) and also exhibits some phenocryst disequilibrium textures (e.g. Table 4 and 6). In Table 10 the compositions of these parental LVF magmas are compared with analyses of primitive lavas from Pacific Rim arc volcanoes.

Using the criteria of Tatsumi & Eggins (1995), who expected primary arc magmas that last equilibrated with peridotite in the mantle wedge to have high *mg*-numbers (≥ 70) and high abundances of compatible trace elements (Ni > 200 ppm, Cr > 400 ppm), none of the LVF lavas, including the parental ones, can be realistically classed as primary. Their *mg*-numbers (<62), Ni (<22 ppm) and Cr (<25 ppm) contents are too low (Table 10), although the *mg*-number is highly dependent on the value of Fe^{3+}/Fe^{2+} used. Two of the PLF2 samples have Ni and Cr contents of ∼60 and ∼150 ppm, respectively, and higher *mg*-numbers (∼71; Table 2), but this is probably a result of *Ol* accumulation in these lavas.

The discrepancy between primitive and parental magma compositions is typically attributed to the prior removal of olivine and/or pyroxene from the latter (e.g. Smith *et al.*, 1997). This seems feasible for the more evolved parental magma (GOO13071; Table 10), but in the case of samples ALA1161 and GRJ288, their low SiO_2 contents would seem to preclude any prior fractionation. It may, therefore, be necessary to invoke crystal accumulation or unusual source and/or melting conditions to explain the peculiar chemistry of these samples.

In addition to low SiO_2, Ni and Cr contents, these lavas also have high TiO_2, Al_2O_3, Fe_2O_3, CaO and low MgO relative to primitive magmas from circum-Pacific arcs (Table 10). Many lavas erupted in arc settings have high Al_2O_3, and they are of sufficient volumetric significance to have spawned the generic term high-Al_2O_3 basalts (HAB). Formal definitions of HAB composition vary, from aphyric basalts with Al_2O_3 >17 wt % (e.g. Tatsumi & Eggins, 1995), to lavas with <54 wt % SiO_2 and >16·5 wt % Al_2O_3 (Crawford *et al.*, 1987), and most

Table 10: Compositions of primitive magmas from Pacific Rim and Sunda arc volcanoes

Arc/region:	Kermadec	Papuan	Luzon	Honshu	Cascade	Aleutian	Mexican	Sunda	LVF	LVF	LVF
Sample no.:	A7125	C33629	SP102	6Z21	MA-696	ID16	22E	86-24b	ALA1161	GRJ288	GOO13071
Analysis:			XRF	XRF	XRF[1]	XRF	WC[2]		XRF	XRF	XRF
Reference:	1	1	2	3	4	5	6	7	This study	This study	This study
SiO_2	49·52	53·42	49·44	49·01	47·5	48·94	49·42	48·5	44·64	43·52	50·69
TiO_2	0·72	1·23	0·84	0·86	1·39	0·70	0·77	1·0	1·51	1·49	1·36
Al_2O_3	17·69	14·53	14·87	18·35	16·9	16·01	16·92	15·7	18·23	17·59	17·29
Fe_2O_3*	10·59	2·83	8·89	3·15	1·96	1·06	4·40	4·2	14·31	14·54	12·50
FeO		4·97		7·19	9·31	7·95	5·30	5·7			
MnO	0·19	0·13	0·16	0·17	0·18	0·17	0·15	0·2	0·19	0·18	0·21
MgO	6·43	8·60	10·88	7·36	8·85	11·42	9·27	10·6	6·40	6·98	4·81
CaO	12·97	7·46	10·17	11·10	10·5	10·89	10·12	11·1	12·68	13·02	8·79
Na_2O	1·31	3·31	2·58	1·48	2·85	2·21	2·49	2·4	2·15	2·03	2·71
K_2O	0·18	1·79	0·87	0·23	0·16	0·52	0·65	0·4	0·64	0·61	1·47
P_2O_5	0·06	0·37	0·22	0·08	0·16	0·12	0·20		0·08	0·07	0·41
Rb	5	33	14	7	3·3	6·6	7	7·7	6·7	7·8	56
Sr	158	670	505	269	247	451	444	369	358	308	384
Y	15	21	13	16	26	16	18		20	19·2	42
Zr	26	214	82	40	98	60	92	59	27	32	180
Nb	0·5	7	6	4	6	2·9	<4		1·7	1·7	6·3
Ba	87	882	277	175	58	231	161	84	283	258	691
Sc	43	20		39	32·9	36·4	35·5	38·1	47	50	34
V	309	162		319	217		196		578	655	311
Cr	116	457	535	87	275	662	378	541	9	25	24
Ni	44	291	223	37	178	266	221	180	8	22	20
Cu	92	27		57	88		24		90	119	158
Zn	71	85		81	85		66		72	77	113
Ga	13	18	9	19			15	4	17	18	19

[1]Nb, V determined by ICP-AES; Sc, Cr, Zn by INAA.
[2]Major elements determined by wet chemical methods; Sc, V, Cr, Ni, Ba by INAA; other trace elements by XRF.
Oxides in wt %, trace elements in ppm. References: 1, Smith *et al.* (1997); 2, Alligator Lake maar, Macolod Corridor, Knittel & Oles (1995); Knittel *et al.* (1997); 3, Zao-san, Gust *et al.* (1997); 4, Mount Adams, Bacon *et al.* (1997); 5, Okmok volcano, Nye & Reid (1986); 6, Tezontal cinder cone, Colima volcano, Luhr & Carmichael (1981); 7, 1982–1983 Galunggung basalt, Gerbe *et al.* (1992).

of the LVF suite satisfy the latter criterion with the exception of several KVT and PLF1/2 samples. However, none of the LVF lavas can be described as aphyric, and indeed, the accumulation of plagioclase phenocrysts in evolved magmas is widely regarded to be the main process of HAB genesis, owing to a significant correlation between Al_2O_3 and modal plagioclase contents in arc volcanic rocks (e.g. Crawford *et al.*, 1987). The modal data for the LVF suite are too limited to identify the presence or absence of any similar correlation (Fig. 18), but it appears that although elevated Al_2O_3 in many of the historical and KVM lavas is clearly related to abundant (>25%) modal *Plag*, the composition of sample ALA1161 ($\sim$9% modal *Plag*) approaches that of a true HAB liquid. However, it could equally be construed as lying within the outer bounds of Crawford *et al.*'s (1987) correlation, so further investigation using REE data and Eu systematics (e.g. Woodhead, 1988), which can discriminate between fractionation and accumulation of plagioclase, would be required to debate this further.

The low SiO_2 contents of samples ALA1161 and GRJ288, and of many other LVF lavas, could also be construed as the result of phenocryst accumulation in more evolved liquids (e.g. Woodhead, 1988). However, if such processes can be discounted, which is possible in the case of sample ALA1161, then other reasons must be sought for the SiO_2 deficiency, in addition to high CaO and Fe_2O_3 (Table 10). Various major elements,

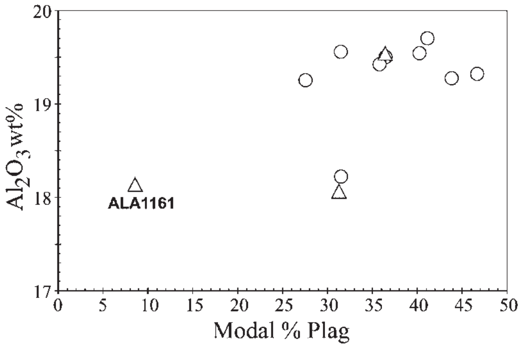

Fig. 18. Whole-rock Al_2O_3 content vs modal % plagioclase (phenocrysts + glomerocrysts only; from Table 3) for selected historical and KVM samples. Symbols as in Fig. 10.

including Si, Fe and Ca, have shown potential as thermometers and barometers in basalts from ocean ridge and arc environments (e.g. Klein & Langmuir, 1987; Plank & Langmuir, 1993). In arc scenarios, high degrees of melting beneath thin arc crust (which allows a more extensive mantle column to undergo decompression melting, assuming melt initiation at a constant depth) are predicted to produce magmas with low Na, and high Ca and Fe (Plank & Langmuir, 1993). This is consistent with the chemistry of the parental LVF lavas (ALA1161 and GRJ288) and thus may be a viable model for magma genesis in the region. Using the expressions of Albarède [1992, equations (2) and (3)], we obtain a temperature of 1220 $\pm$ 40 °C and a pressure of 15·5 $\pm$ 2·7 kbar for a primary mantle melt with SiO_2 and MgO contents equivalent to ALA1161, although this is based on fluid-absent melting experiments. These conditions are similar to those obtained experimentally by Tatsumi *et al.* (1983) for the segregation of arc HAB from its source (15 kbar, 1340 °C under anhydrous conditions; 17 kbar, 1325 °C with 1·5 wt % H_2O in the melt). Such temperatures are postulated to be excessively high for a stable mantle geotherm in a subduction zone, and are believed to demonstrate the existence of mantle diapirs beneath some arc volcanoes (e.g. Tatsumi *et al.*, 1983).

Contents of V, and to a lesser extent Sc, in samples ALA1161 and GRJ288 are also high in comparison with primitive arc magmas (Table 10), although the low SiO_2 contents of the LVF lavas make intercomparison difficult. V and Sc are particularly compatible in clinopyroxene, magnetite and amphibole, but the latter is considered to have the strongest affinity for these elements in basaltic liquids (e.g. Vukadinovic & Sutawidjaja, 1995). Although the effects of clinopyroxene accumulation cannot be ruled out, an alternative explanation for elevated V and Sc in these lavas is that the source region was abnormally rich in pyroxene or amphibole. Sisson & Bronto (1998) have recently inferred the involvement of pyroxenitic rocks in magma genesis at Galunggung volcano in West Java, in conjunction with a mantle diapir model similar to that propounded by Tatsumi *et al.* (1983). Low-degree melts of these pyroxene-rich lithologies entrained in upwelling mantle produce SiO_2-undersaturated liquids with low H_2O concentrations (Sisson & Bronto, 1998).

DISCUSSION

Probably the most enigmatic aspect of the LVF is the occurrence of parental lavas, related both to the back-arc volcano, Bromo, and the arc-front volcano, Semeru, at similar distances from the trench. Furthermore, although Lamongan is in roughly the same position with respect to the trench as Bromo (Fig. 1), the historical and youngest prehistoric products of the volcano are medium-K basalts and basaltic andesites that can be genetically related to lavas currently erupting from Semeru. It is therefore likely that the two volcanoes are supplied by a common parental magma, of a composition similar to ALA1161 or GRJ288, and that these parental liquids are erupted as cinder cones in the LVF as a result of peculiar regional tectonics (see below).

The origin of the high-K cinder cones in the western LVF is unclear, but given their parental relationship to lavas from Bromo, it is possible that they represent the products of volcanism on the periphery of the Bromo–Tengger complex. These cones are amongst the oldest in the LVF and hence may not be temporally associated with activity in the rest of the field. However, geochronological work is needed to fully establish the age relationships between the various groups of vents identified in this study.

A working model for magma genesis beneath the LVF can be proposed, based on the salient geochemical features of the erupted lavas. It is stressed that this is probably only one of several possible models, but it is one that follows recent research on magma genesis at Javanese volcanoes (Sisson & Bronto, 1998) and that is broadly consistent with the LVF data. In this model, mantle upwelling and pressure-release melting occurs beneath the LVF. If extensional tectonics predominates in this part of East Java (as suggested by recent seismic crises in the LVF), the crust may be locally relatively thin, and thus high melt fractions can be achieved through the melting of hot, upwelling mantle. This produces primary HAB magmas with low SiO_2 (if melting begins at high pressures) and Na_2O and high CaO, FeO and Al_2O_3, which fractionate *Ol*, *Cpx* and calcic *Plag* during ascent to produce low-Mg HAB. Upon reaching the base of the crust small batches of this magma exploit extensional fractures and penetrate to the surface to erupt as cinder cones (e.g. ALA1161) or possibly maars; the rest may pond and fractionate further, or intrude into the crust and supply a small crustal magma chamber beneath the main volcanic edifice. The location of magma chamber formation, and hence of the LTT edifice in the LVF, may be controlled by the intersection of regional faults (Carn, 2000). Evolution in the magma chamber involves further fractionation of *Ol*, *Cpx*, *Plag*, *Mag* and minor *Opx*, along with the accumulation and resorption of phenocrysts. As fractionation proceeds, the residual liquid becomes increasingly volatile rich, until saturation is reached and exsolution of bubbles begins; this may trigger a phase of rapid growth of cellular *Plag* on pre-existing phenocrysts. Continuing exsolution increases the chamber pressure until eruption occurs, with crustal faults and fractures that intersect the chamber, possibly at deeper levels, acting as conduits for flank cinder cone and perhaps fissure-style eruptions (e.g. the KVM cones). The PLF2, PLF3 and historical lavas in the LVF are all interpreted as products of flank or summit eruptions from the LTT edifice supplied by a sub-volcanic chamber.

The KVT cones and PLF1 flows are assumed to represent an earlier phase of volcanism associated with the Tengger caldera, possibly before the initiation of regional extension and local thinning of the crust. This could explain the observed juxtaposition of 'back-arc' and 'fore-arc' magmas in the LVF. The chemical similarity between many of the maar deposits and the KVT–PLF1 samples (e.g. Fig. 10) suggests that the maar-forming eruptions often included fragments of the PLF1 flows as lithic material.

The compositionally distinct group of cones to the NE of Klakah (Fig. 2) could be the result of small-scale source heterogeneity, in conjunction with local fractures to convey the magmas to the surface whilst preserving their individuality. This is supported by the observation that these cones appear to vary considerably in age. Fracturing during the recent seismic crises in the LVF was concentrated in this region (Matahelumual, 1990). More detailed isotopic data from the LVF are needed to shed further light on this aspect of the complex. However, it is clear that spatial variations in source characteristics can be identified only where there is spatial variation in vent locations (i.e. in volcanic fields).

Although the regional tectonic framework of East Java is poorly known, it is clear that the LVF must occupy a zone of crustal extension. The existence of a monogenetic vent complex, the locally 'pinched out' topography of the island and the formation of the back-arc Madura Basin to the north (Fig. 1) all suggest an extensional regime. The LVF is also significant as it marks one of several locations on Java where the volcanic front is displaced away from the trench (Fig. 1). Gunung Slamet, a volcano in central Java, occupies a similar location and shares several structural characteristics with Lamongan (e.g. Vukadinovic & Sutawidjaja, 1995). Its central edifice also comprises two eruptive centres, split by a NW–SE-trending breach (similar to LTT; Figs 2 and 3), and it also has a scoria cone field on its flanks. These features may relate to the large-scale segmentation of the subduction system along this portion of the Sunda arc, with the LVF and Slamet situated at the boundaries of arc segments (Carn *et al.*, in preparation).

SUMMARY

Initial activity in the LVF may have involved the eruption of high-K back-arc basalts parental to the current products of the Bromo–Tengger system, in what is now the western part of the field. Subsequent or continuing extension perpendicular to the arc in East Java locally thinned the crust, and altered the composition of erupted lavas, producing low-Mg HAB. Exploitation of extensional fractures in the crust by small batches of rising magma led to the development of a cinder cone and maar field, and ultimately to the growth of a basaltic stratovolcano (LTT; estimated age $\sim$13–40 ka) at the intersection of two or more major lines of weakness in the crust. The magma chamber beneath LTT fed further cinder cone eruptions and crystal-rich lava flows on the immediate flanks of the volcano. However, the most primitive lavas exposed in the LVF are associated with some of the youngest prehistoric cinder cones, indicating relatively recent supply of new magma to the system. Extensional tectonics is still active in the LVF, as testified by the formation of ENE–WSW and east–west tensional fissures during the 20th-century seismic crises.

ACKNOWLEDGEMENTS

We thank John Watson and Pete Webb at the Department of Earth Sciences, Open University, for assistance with XRF analyses. Hazel Chapman, Judith Bunbury, Maurice Haslop, Dave Newling and Stephen Reed (Cambridge) are gratefully acknowledged for guidance in Sr isotopic analysis, electron microprobe work and sample preparation. Fieldwork in Java was assisted by staff of the Volcanological Survey of Indonesia (VSI) from Bandung (Dedi Kusnadi), Yogyakarta (Dewi Subektiningsih) and Klakah (Sugeng Santosa, Bambang Wibono). We acknowledge helpful reviews by Ulrich Knittel and John Foden. S.A.C. was supported by a research studentship from the UK Natural Environment Research Council (GT4/94/137/G).

REFERENCES

Albarède, F. (1992). How deep do common basaltic magmas form and differentiate? *Journal of Geophysical Research* **97**, 10997–11009.

Albarède, F. (1995). *Introduction to Geochemical Modelling.* Cambridge: Cambridge University Press.

Albarède, F., Luais, B., Fitton, G., Semet, M., Kaminski, E., Upton, B. G. J., Bachèlery, P. & Cheminée, J.-L. (1997). The geochemical regimes of Piton de la Fournaise volcano (Réunion) during the last 530 000 years. *Journal of Petrology* **38**, 171–201.

Apperson, K. D. (1991). Stress fields of the overriding plate at convergent margins and beneath active volcanic arcs. *Science* **254**, 670–678.

Bacon, C. R., Bruggman, P. E., Christiansen, R. L., Clynne, M. A., Donnelly-Nolan, J. M. & Hildreth, W. (1997). Primitive magmas at five Cascade volcanic fields: melts from hot, heterogeneous sub-arc mantle. *Canadian Mineralogist* **35**, 397–423.

Borg, L. E., Clynne, M. A. & Bullen, T. D. (1997). The variable role of slab-derived fluids in the generation of a suite of primitive calc-alkaline lavas from the southernmost Cascades, California. *Canadian Mineralogist* **35**, 425–452.

Bronto, S., Situmorang, T. & Effendi, W. (1986). *Geologic map of Lamongan volcano, Lumajang, East Java*. Bandung: Volcanological Survey of Indonesia.

Bryan, W. B., Finger, L. W. & Chayes, F. (1969). Estimating proportions in petrographic mixing equations by least-squares approximation. *Science* **163**, 926–927.

Campbell, I. H., Roeder, P. L. & Dixon, J. M. (1978). Plagioclase buoyancy in basaltic liquids as determined with a centrifuge furnace. *Contributions to Mineralogy and Petrology* **67**, 369–377.

Camus, G., Gourgaud, A. & Vincent, P. M. (1987). Petrologic evolution of Krakatau (Indonesia): implications for a future activity. *Journal of Volcanology and Geothermal Research* **33**, 299–316.

Carn, S. A. (1999). Application of synthetic aperture radar (SAR) imagery to volcano mapping in the humid tropics: a case study in East Java, Indonesia. *Bulletin of Volcanology* **61**, 92–105.

Carn, S. A. (2000). The Lamongan volcanic field, East Java, Indonesia: physical volcanology, historic activity and hazards. *Journal of Volcanology and Geothermal Research* **95**, 81–108.

Charlton, T. R. (1991). Postcollision extension in arc–continent collision zones, eastern Indonesia. *Geology* **19**, 28–31.

Chesner, C. A. (1998). Petrogenesis of the Toba Tuffs, Sumatra, Indonesia. *Journal of Petrology* **39**, 397–438.

Chotin, P., Giret, A., Rampnoux, J.-P., Sumarso, & Suminta (1980). L'île de Java, un enregistreur des mouvements tectoniques à l'aplomb d'une zone de subduction. *Compte Rendu Sommaire des Séances de la Société Géologique de France* **5**, 175–177.

Crawford, A. J., Falloon, T. J. & Eggins, S. (1987). The origin of island arc high-alumina basalts. *Contributions to Mineralogy and Petrology* **97**, 417–430.

Defant, M. J. & Nielsen, R. L. (1990). Interpretation of open system petrogenetic processes: phase equilibria constraints on magma evolution. *Geochimica et Cosmochimica Acta* **54**, 87–102.

Dickinson, W. R. (1975). Potassium–depth (K–h) relations in continental margin and intraoceanic magmatic arcs. *Geology* **3**, 53–56.

Dunn, T. & Sen, C. (1994). Mineral/matrix partition-coefficients for orthopyroxene, plagioclase, and olivine in basaltic to andesitic systems—a combined analytical and experimental study. *Geochimica et Cosmochimica Acta* **58**, 717–733.

Edwards, C. M. H., Morris, J. D. & Thirlwall, M. F. (1993). Separating mantle from slab signatures in arc lavas using B/Be and radiogenic isotope systematics. *Nature* **362**, 530–533.

Edwards, C. M. H., Menzies, M. A., Thirlwall, M. F., Morris, J. D., Leeman, W. P. & Harmon, R. S. (1994). The transition to potassic alkaline volcanism in island arcs: the Ringgit–Beser complex, East Java, Indonesia. *Journal of Petrology* **35**, 1557–1595.

Foden, J. D. (1983). The petrology of the calc-alkaline lavas of Rindjani volcano, east Sunda Arc: a model for island arc petrogenesis. *Journal of Petrology* **24**, 98–130.

Foden, J. D. & Varne, R. (1980). The petrology and tectonic setting of Quaternary–Recent volcanic centres of Lombok and Sumbawa, Sunda Arc. *Chemical Geology* **30**, 201–226.

Gerbe, M.-C., Gourgaud, A., Sigmarsson, O., Harmon, R. S., Joron, J.-L. & Provost, A. (1992). Mineralogical and geochemical evolution of the 1982–1983 Galunggung eruption (Indonesia). *Bulletin of Volcanology* **54**, 284–298.

Gust, D. A., Arculus, R. J. & Kersting, A. B. (1997). Aspects of magma sources and processes in the Honshu arc. *Canadian Mineralogist* **35**, 347–365.

Hamilton, W. (1979). Tectonics of the Indonesian Region. *US Geological Survey Professional Paper* **1078**.

Hamilton, W. B. (1988). Plate tectonics and island arcs. *Geological Society of America Bulletin* **100**, 1503–1527.

Hutchison, C. S. (1982). Indonesia. In: Thorpe, R. S. (ed.) *Andesites: Orogenic Andesites and Related Rocks*. New York: John Wiley, pp. 207–224.

Irvine, T. N. & Baragar, W. R. A. (1971). A guide to the chemical classification of the common volcanic rocks. *Canadian Journal of Earth Sciences* **8**, 523–548.

Jeffries, T. E., Perkins, W. T. & Pearce, N. J. G. (1995). Measurements of trace-elements in basalts and their phenocrysts by laser probe microanalysis inductively-coupled plasma-mass spectrometry (LPMA-ICP-MS). *Chemical Geology* **121**, 131–144.

Jurewicz, A. J. G. & Watson, E. B. (1988). Cations in olivine, part 1: calcium partitioning and calcium–magnesium distribution between olivines and coexisting melts, with petrologic applications. *Contributions to Mineralogy and Petrology* **99**, 176–185.

Katili, J. A. (1975). Volcanism and plate tectonics in the Indonesian island arcs. *Tectonophysics* **26**, 165–188.

Klein, E. M. & Langmuir, C. H. (1987). Global correlations of ocean ridge basalt chemistry with axial depth and crustal thickness. *Journal of Geophysical Research* **92**, 8089–8115.

Knittel, U. & Oles, D. (1995). Basaltic volcanism associated with extensional tectonics in the Taiwan–Luzon island arc: evidence for non-depleted sources and subduction zone enrichment. In: Smellie, J. L. (ed.) *Volcanism Associated with Extension at Consuming Plate Margins. Geological Society, London, Special Publications* **81**, 77–93.

Knittel, U., Hegner, E., Bau, M. & Satir, M. (1997). Enrichment processes in the sub-arc mantle: a Sr–Nd–Pb isotopic and REE study of primitive arc basalts from the Philippines. *Canadian Mineralogist* **35**, 327–346.

Kuno, H. (1968). Differentiation of basalt magmas. In: Hess, H. H. & Poldervaart, A. (eds) *Basalts: the Poldervaart Treatise on Rocks of Basaltic Composition, Vol. 2*. New York: Interscience, pp. 623–688.

Le Bas, M. J., Le Maitre, R. W., Streckeisen, A. & Zanettin, B. (1986). A chemical classification of volcanic rocks based on the Total Alkali–Silica diagram. *Journal of Petrology* **27**, 745–750.

Le Maitre, R. W. (1968). Chemical variation within and between volcanic rock series—a statistical approach. *Journal of Petrology* **9**, 220–252.

Leterrier, J., Yuwono, Y. S., Soeria-Atmadja, R. & Maury, R. C. (1990). Potassic volcanism in Central Java and South Sulawesi, Indonesia. *Journal of Southeast Asian Earth Sciences* **4**, 171–187.

Lindsley, D. H. (1983). Pyroxene thermometry. *American Mineralogist* **68**, 477–493.

Luhr, J. F. (1997). Extensional tectonics and the diverse primitive volcanic rocks in the western Mexican volcanic belt. *Canadian Mineralogist* **35**, 473–500.

Luhr, J. F. & Carmichael, I. S. E. (1981). The Colima volcanic complex, Mexico: Part II. Late Quaternary cinder cones. *Contributions to Mineralogy and Petrology* **76**, 127–147.

Mandeville, C. W., Carey, S. & Sigurdsson, H. (1996). Magma mixing, fractional crystallization and volatile degassing during the 1883 eruption of Krakatau volcano, Indonesia. *Journal of Volcanology and Geothermal Research* **74**, 243–274.
Matahelumual, J. (1990). Gunung Lamongan. *Berita Berkala Vulkanologi, Edisi Khusus No. 125* (in Indonesian). Bandung: Volcanological Survey of Indonesia.
Morrice, M. G. & Gill, J. B. (1986). Spatial patterns in the mineralogy of island arc magma series: Sangihe arc, Indonesia. *Journal of Volcanology and Geothermal Research* **29**, 311–353.
Mulyana, R. (1989). Pétrologie et géochimie du volcan Lamongan, Java–Indonesie. DEA thesis, Université de Bretagne Occidentale, Brest.
Nicholls, I. A. & Whitford, D. J. (1976). Primary magmas associated with Quaternary volcanism in the western Sunda Arc, Indonesia. In: Johnson, R. W. (ed.) *Volcanism in Australasia*. Amsterdam: Elsevier, pp. 77–90.
Nicholls, I. A. & Whitford, D. J. (1983). Potassium-rich volcanic rocks of the Muriah complex, Java, Indonesia: products of multiple magma sources? *Journal of Volcanology and Geothermal Research* **18**, 337–359.
Nye, C. J. & Reid, M. R. (1986). Geochemistry of primary and least fractionated lavas from Okmok volcano, Central Aleutians: implications for arc magmagenesis. *Journal of Geophysical Research* **91**, 10271–10287.
Panjasawatwong, Y., Danyushevsky, L. V., Crawford, A. J. & Harris, K. L. (1995). An experimental study of the effects of melt composition on plagioclase–melt equilibria at 5 and 10 kbar: implications for the origin of magmatic high-An plagioclase. *Contributions to Mineralogy and Petrology* **118**, 420–432.
Pearce, J. A. & Peate, D. W. (1995). Tectonic implications of the composition of volcanic arc magmas. *Annual Review of Earth and Planetary Sciences* **23**, 251–285.
Peccerillo, A. & Taylor, S. R. (1976). Geochemistry of Eocene calc-alkaline volcanic rocks from the Kastamonu area, northern Turkey. *Contributions to Mineralogy and Petrology* **58**, 63–81.
Plank, T. & Langmuir, C. H. (1993). Tracing trace elements from sediment input to volcanic output at subduction zones. *Nature* **362**, 739–743.
Puspito, N. T. & Shimazaki, K. (1995). Mantle structure and seismotectonics of the Sunda and Banda arcs. *Tectonophysics* **251**, 215–228.
Rangin, C., Jolivet, L., Pubellier, M., Azéma, J., Briais, A., Chotin, P., Fontaine, H., Huchon, P., Maury, R., Müller, C., Rampnoux, J. P., Stephan, J. F. & Tournon, J. (1990). A simple model for the tectonic evolution of southeast Asia and Indonesia region for the past 43 m.y. *Bulletin de la Société Géologique de France* **8**, 889–905.
Rickwood, P. C. (1989). Boundary lines within petrological diagrams which use oxides of major and minor elements. *Lithos* **22**, 247–263.
Roeder, P. L. & Emslie, R. F. (1970). Olivine–liquid equilibrium. *Contributions to Mineralogy and Petrology* **29**, 275–289.
Said, H. (1992). Gunung Lamongan. *Berita Berkala Vulkanologi, Edisi Khusus No. 175* (in Indonesian). Bandung: Volcanological Survey of Indonesia.
Self, S., Rampino, M. R., Newton, M. S. & Wolff, J. A. (1984). Volcanological study of the great Tambora eruption of 1815. *Geology* **12**, 659–663.
Self, S. & King, A. J. (1996). Petrology and sulfur and chlorine emissions of the 1963 eruption of Gunung Agung, Bali, Indonesia. *Bulletin of Volcanology* **58**, 263–285.
Seyler, M. & Bonatti, E. (1994). Na, Al^{IV} and Al^{VI} in clinopyroxenes of subcontinental and suboceanic ridge peridotites: a clue to different melting processes in the mantle? *Earth and Planetary Science Letters* **122**, 281–289.
Shaw, D. M. (1970). Trace element fractionation during anatexis. *Geochimica et Cosmochimica Acta* **34**, 237–243.
Silver, E. A., Reed, D. & McCaffrey, R. (1983). Back arc thrusting in the eastern Sunda arc, Indonesia: a consequence of arc–continent collision. *Journal of Geophysical Research* **88**, 7429–7448.
Simkin, T. & Siebert, L. (1994). *Volcanoes of the World*, 2nd edn. Tucson, AZ: Geoscience Press.
Sisson, T. W. & Bronto, S. (1998). Evidence for pressure-release melting beneath magmatic arcs from basalt at Galunggung, Indonesia. *Nature* **391**, 883–886.
Skogby, H. (1994). OH incorporation in synthetic clinopyroxene. *American Mineralogist* **79**, 240–249.
Smith, I. E. M., Worthington, T. J., Price, R. C. & Gamble, J. A. (1997). Primitive magmas in arc-type volcanic associations: examples from the Southwest Pacific. *Canadian Mineralogist* **35**, 257–273.
Soeria-Atmadja, R., Maury, R. C., Bellon, H., Pringgoprawiro, H., Polve, M. & Priad, B. (1994). Tertiary magmatic belts in Java. *Journal of Southeast Asian Earth Sciences* **9**, 13–27.
Stolz, A. J., Varne, R., Wheller, G. E., Foden, J. D. & Abbott, M. J. (1988). The geochemistry and petrogenesis of K-rich alkaline volcanics from the Batu Tara volcano, eastern Sunda Arc. *Contributions to Mineralogy and Petrology* **98**, 374–389.
Stolz, A. J., Varne, R., Davies, G. R., Wheller, G. E. & Foden, J. D. (1990). Magma source components in an arc–continent collision zone: the Flores–Lembata sector, Sunda Arc, Indonesia. *Contributions to Mineralogy and Petrology* **105**, 585–601.
Sun, S.-S. & McDonough, W. F. (1989). Chemical and isotopic systematics of oceanic basalts: implications for mantle compositions and processes. In: Saunders, A. D. & Norry, M. J. (eds) *Magmatism in the Ocean Basins. Geological Society, London, Special Publications* **42**, 313–345.
Tatsumi, Y. & Eggins, S. (1995). *Subduction Zone Magmatism*. Cambridge, MA: Blackwell Science.
Tatsumi, Y., Sakuyama, M., Fukuyama, H. & Kushiro, I. (1983). Generation of arc basalt magmas and thermal structure of the mantle wedge in subduction zones. *Journal of Geophysical Research* **88**, 5815–5825.
Tatsumi, Y., Hamilton, D. L. & Nesbitt, R. W. (1986). Chemical characteristics of fluid phase released from a subducted lithosphere and the origin of arc magmas: evidence from high pressure experiments and natural rocks. *Journal of Volcanology and Geothermal Research* **29**, 293–309.
Tsuchiyama, A. (1985). Dissolution kinetics of plagioclase in the melt of the system diopside–albite–anorthite, and origin of dusty plagioclase in andesites. *Contributions to Mineralogy and Petrology* **89**, 1–16.
Ulmer, P. (1989). The dependence of the Fe^{2+}–Mg cation-partitioning between olivine and basaltic liquid on pressure, temperature and composition. *Contributions to Mineralogy and Petrology* **101**, 261–273.
Van Bergen, M. J., Erfan, R. D., Sriwana, T., Suharyono, K., Poorter, R. P. E., Varekamp, J. C., Vroon, P. Z. & Wirakusumah, A. D. (1989). Spatial geochemical variations of arc volcanism around the Banda Sea. *Netherlands Journal of Sea Research* **24**, 313–322.
Van Gerven, M. & Pichler, H. (1995). Some aspects of the volcanology and geochemistry of the Tengger Caldera, Java, Indonesia: eruption of a K-rich tholeiitic series. *Journal of Southeast Asian Earth Sciences* **11**, 125–133.
Varekamp, J. C., Van Bergen, M. J., Vroon, P. Z., Poorter, R. P. E., Wirakusumah, A. D., Erfan, R. D., Suharyono, K. & Sriwana, T. (1989). Volcanism and tectonics in the eastern Sunda arc, Indonesia. *Netherlands Journal of Sea Research* **24**, 303–312.
Varne, R. (1985). Ancient subcontinental mantle: a source for K-rich orogenic volcanics. *Geology* **13**, 405–408.

Villemant, B., Jaffrezic, H., Joron, J. L. & Treuil, M. (1981). Distribution coefficients of major and trace-elements—fractional crystallization in the alkali basalt series of Chaîne-des-Puys (Massif Central, France). *Geochimica et Cosmochimica Acta* **45**, 1997–2016.

Vukadinovic, D. (1993). Are Sr enrichments in arc basalts due to plagioclase accumulation? *Geology* **21**, 611–614.

Vukadinovic, D. (1995). High-field-strength elements in Javanese arc basalts and chemical layering in the mantle wedge. *Mineralogy and Petrology* **55**, 293–308.

Vukadinovic, D. & Nicholls, I. A. (1989). The petrogenesis of island arc basalts from Gunung Slamet volcano, Indonesia: trace element and $^{87}Sr/^{86}Sr$ constraints. *Geochimica et Cosmochimica Acta* **53**, 2349–2363.

Vukadinovic, D. & Sutawidjaja, I. (1995). Geology, mineralogy and magma evolution of Gunung Slamet volcano, Java, Indonesia. *Journal of Southeast Asian Earth Sciences* **11**, 135–164.

Wahyudin, D. (1991). Volcanology and petrology of Mt. Semeru volcanic complex, East Java–Indonesia. M.Sc thesis, Victoria University, Wellington.

Wheller, G. E. & Varne, R. (1986). Genesis of dacitic magmatism at Batur volcano, Bali, Indonesia: implications for the origins of stratovolcano calderas. *Journal of Volcanology and Geothermal Research* **28**, 363–378.

Wheller, G. E., Varne, R., Foden, J. D. & Abbott, M. J. (1987). Geochemistry of Quaternary volcanism in the Sunda–Banda Arc, Indonesia, and three-component genesis of island arc basaltic magmas. *Journal of Volcanology and Geothermal Research* **32**, 137–160.

Whitford, D. J. (1975). Strontium isotopic studies of the volcanic rocks of the Sunda Arc, Indonesia, and their petrogenetic implications. *Geochimica et Cosmochimica Acta* **39**, 1287–1302.

Whitford, D. J. & Nicholls, I. A. (1976). Potassium variations in lavas across the Sunda arc in Java and Bali. In: Johnson, R. W. (ed.) *Volcanism in Australasia*. Amsterdam: Elsevier, pp. 63–75.

Whitford, D. J., Nicholls, I. A. & Taylor, S. R. (1979). Spatial variations in the geochemistry of Quaternary lavas across the Sunda Arc in Java and Bali. *Contributions to Mineralogy and Petrology* **70**, 341–356.

Whitford, D. J., White, W. M. & Jezek, P. A. (1981). Neodymium isotopic composition of Quaternary island arc lavas from Indonesia. *Geochimica et Cosmochimica Acta* **45**, 989–995.

Widiyantoro, S. & van der Hilst, R. (1996). Structure and evolution of lithospheric slab beneath the Sunda arc, Indonesia. *Science* **271**, 1566–1570.

Widiyantoro, S. & van der Hilst, R. (1997). Mantle structure beneath Indonesia inferred from high-resolution tomographic imaging. *Geophysical Journal International* **130**, 167–182.

Wood, C. P., Nairn, I. A., Mckee, C. O. & Talai, B. (1995). Petrology of the Rabaul Caldera area, Papua New Guinea. *Journal of Volcanology and Geothermal Research* **69**, 285–302.

Woodhead, J. D. (1988). The origin of geochemical variations in Mariana lavas: a general model for petrogenesis in intra-oceanic island arcs? *Journal of Petrology* **29**, 805–830.